FINAL TECHNICAL REPORT

Quantifying Surface Fault Rupture Location Uncertainty for Lifeline Crossings

Recipient:

California Geological Survey
801 K Street, MS 12-32
Sacramento, CA 95814-3530
Tel (916) 322-9317; Fax (916) 322-4765; URL www.consrv.ca.gov/CGS

Principal Investigators:

Rui Chen
Rui.Chen@conservation.ca.gov

Timothy E. Dawson
Timothy.Dawson@conservation.ca.gov

Chris J. Wills
Chris.Wills@conservation.ca.gov

Keywords:
Surface fault rupture, location uncertainty, probabilistic fault displacement hazard analysis.

Program Elements I and III

U. S. Geological Survey
National Earthquake Hazards Reduction Program
Award Number G11AP20040
(from January 1, 2011 to December 31, 2012)

March 2013

Research supported by the U.S. Geological Survey (USGS), Department of the Interior, under USGS award number G11AP20040. The views and conclusions contained in this document are those of the authors and should not be interpreted as necessarily representing the official policies, either expressed or implied, of the U.S. Government.

EXECUTIVE SUMMARY

Many vital lifelines, such as transportation bridges, roads, utilities, and communication lines have suffered significant damage due to surface fault displacement associated with large earthquakes. Prime examples of significant lifeline disruptions are provided by the 1999 Turkey (M7.4 Kocaeli and M7.2 Duzce), 1999 Taiwan (M7.6 Chi-Chi), and the 2008 China (M7.9 Wenchuan) earthquakes. It is possible to reduce lifeline structural damage and the associated business and social disruption where potential surface fault rupture is unavoidable if fault displacement hazards can be incorporated in the design of lifeline infrastructure. Incorporating fault displacement hazards in structural design requires quantitative estimates of fault displacement hazards. General methods have been developed in recent years to analyze fault displacement hazards using a probabilistic approach. Probabilistic fault displacement hazard analyses (PFDHA) rely on regression relations that are functions of the accuracy of fault mapping, the complexity of the mapped fault traces, the foundation footprint size of structures under consideration, and surface fault displacement data measured around mapped faults. Application of these methods and regressions suggests that location uncertainty in surface rupture plays an important role, and the treatment of location uncertainty constitutes an essential part of PFDHA. There are two components of location uncertainty: uncertainty associated with the accuracy of existing mapped fault traces (epistemic uncertainty), and natural variability in the location of possible/potential surface rupture from future earthquakes around a previously existing, precisely located earthquake fault (aleatory variability). Separating aleatory variability from epistemic uncertainty is the main objective of this study.

We demonstrate a GIS-based approach to develop necessary data to quantify location uncertainty associated with existing fault maps. We choose the published Alquist-Priolo (AP) Earthquake Fault Zone maps as our existing fault maps because these AP maps are widely distributed and routinely referenced in engineering practice in California. Improved surface fault traces are obtained by careful interpretation of surface fault features using high-resolution LiDAR digital elevation models (DEM) and other imagery. A statistically robust dataset is developed for the AP maps by systematically measuring the distances between improved fault traces and existing AP fault traces. Summary statistics of this dataset indicate that the locations of surface ruptures for accurately mapped, approximately mapped, concealed, and inferred fault traces have standard deviations of 23 m, 36 m, 44 m, and 45 m, respectively. The likely extent of occurrence of future surface rupture can be estimated for a chosen probability level from these simple statistics. For example, there is about 95% probability that surface rupture from future earthquakes would occur within about 46 m (i.e., two standard deviations) on either side of an accurately mapped fault if we assume a normal distribution of epistemic location uncertainty.

To better understand whether and how aleatory variability can be quantified, we analyze trenches documented in paleoseismic literature, particularly trenches exposing evidence for paleoseismic events. In addition, we re-analyze numerous trench logs from decades of fault investigations for research and development projects throughout California. We measure the total width of surface faulting revealed in these trenches and determine distances from the most recent event to prior events when such information is available. We compile the measured data to quantify the natural variability part of surface rupture location uncertainty. We are unable to define a statistical distribution for aleatory location uncertainty with reasonable confidence due to data limitation. However, we estimate its upper and lower bound standard deviations to be approximately 14 m and 37 m, respectively, on either side of a mapped fault.

We modify the numerical algorithms in our PFDHA code to treat aleatory variability and epistemic uncertainty separately. A simple example shows the strong effect of location uncertainty on the estimated probabilistic rupture displacement. Large uncertainties for poorly mapped faults correspond to wide displacement profiles across mapped faults. Improving fault mapping using publically available LiDAR DEMs and other imagery can reduce epistemic uncertainty. We demonstrate that such precise mapping efforts can reduce the width of an estimated displacement profile by 67% to 69% to the lower bound aleatory variability and 16% to 19% to the upper bound aleatory uncertainty for the concealed and inferred categories, respectively. For the accurately and approximately located fault trace categories, the estimated displacement zone width is reduced by 37% and 60%, respectively, to the lower bound aleatory variability. The upper bound aleatory variability has a standard deviation similar to that of the approximately mapped fault trace category and larger than the standard deviation of the accurately mapped fault trace category. We hope to narrow the estimates of aleatory location variability with additional trench data, particularly data from trenches that expose evidence of multiple paleoseismic events.

TABLE OF CONTENTS

Executive Summary ii
Table of Contents iv
Introduction 1
Surface Fault Rupture Location Uncertainty 3
Data Acquisition Methodology 4
First Group of Location Uncertainty Data 5
Second Group of Location Uncertainty Data 6
Third Group of Location Uncertainty Data 6
Summary of Location Uncertainty Data Statistics 7
Previously Unmapped Traces 7
Surface Rupture Location Variability 8
Data Availability 8
Compilation of Paleoseismic Data 8
Location Variability Data Analysis and Statistics 9
Data Limitations 10
Implementation of Rupture Location Uncertainty and Variabilty in PFDHA 11
Implementation in PFDHA 12
Example Applications 13
Discussion and Conclusions 14
Acknowledgements 15
References 15
Tables and Figures 18

INTRODUCTION

Surface fault displacement associated with large earthquakes has caused significant damage to community infrastructure. As a direct result of the extensive damage to homes, commercial buildings, and other structures due to surface rupture associated with the 1971 M6.6 San Fernando earthquake, the State of California established the Alquist-Priolo (AP) Earthquake Fault Zoning Act to mitigate hazards of surface faulting to structures for human occupancy (http://www.consrv.ca.gov/cgs/rghm/ap/Pages/main.aspx). Destructive damage to vital lifeline infrastructure caused by surface rupture occurred in most recent large earthquakes, including the 1999 Chi-Chi M7.6 earthquake in Taiwan (Kawashima, 2002; Lien, 1999), the 1999 M7.2 Kocaeli and M7.2 Duzce earthquakes in Turkey (Pamuk et al., 2005), and the 2008 Wenchuan M7.9 earthquake in China (Xu et al., 2008; Liu, 2008).

It is possible to reduce lifeline structural damage and associated business and social disruption if fault displacement hazards can be incorporated in structural design. For example, the Trans-Alaska Pipeline was designed to accommodate large surface fault displacement and consequently survived approximately 5.5 meters of fault displacement produced by the M7.9 Denali Earthquake (Hall et al., 2003). Incorporating fault displacement hazards requires quantitative estimates of the hazards. Although federal, state, and local governments regulate the construction of buildings, lifelines and other critical infrastructure on active faults, there are no standards for the quantitative evaluation of fault displacement, or for structural design that incorporates fault displacement hazards. Improving our understanding and estimates of displacement hazards at lifeline fault crossings will contribute to reduction of earthquake losses associated with damage to these lifeline structures.

Youngs et al. (2003) established a general methodology for probabilistic fault displacement hazard analysis (PFDHA) and developed probability distributions for normal faults. Petersen et al. (2011) extended the Youngs et al. (2003) earthquake approach to strike-slip faults and developed equations to account for mapping accuracy and fault complexity parameters, as well as the footprint size of structures to be placed at the site of interest. Numerous large historical earthquakes show that surface ruptures are not always located on the fault traces mapped prior to the earthquake. In some cases, there is considerable uncertainty in rupture location. In the Petersen et al. (2011) methodology, location uncertainty is incorporated and characterized by a probability distribution of measured distances between the locations of the surface ruptures of large historical earthquakes and the mapped locations of the corresponding earthquake faults. That study used hundreds of observations comparing locations of mapped faults to the rupture traces from nine global strike-slip earthquakes ranging from M6.5 to M7.6. Separate data sets were obtained and regressed for the four categories of mapping accuracy used in the AP fault maps, namely, “accurately located,” “approximately located,” “inferred,” and “concealed” fault traces. The inferred and concealed fault traces were further categorized as “simple” and “complex” traces, based on whether or not the fault has a geometric complexity, such as a step over. The location uncertainty data were assumed to follow a normal distribution centered at the mapped earthquake fault. Table 1 shows the summary statistics of location uncertainty data from historical earthquakes. In all tables in this report, σ is standard deviation and COV is coefficient of variation. In hazard calculations, location uncertainty is integrated to two standard deviations on either side of the fault. Consequently, the calculated displacement for a given hazard level at a given location is a bell-shaped profile that is

perpendicular to the fault strike and centered on the mapped fault trace. Figure 1 shows the strong effect of location uncertainty on the calculated hazard. As indicated in Table 1, accurately mapped traces have a standard deviation of about 27 m. However, the inferred traces have standard deviations almost three times as large. This higher uncertainty translates into increased hazard at distances beyond 100 m (Figure 1a). Complex fault traces that are inferred or concealed have even larger uncertainty, with a standard deviation of about 116 m. This large uncertainty translates into significant displacements at distances of a few hundred meters from the mapped fault. Figure 1(b) shows that for the 10% probability of exceedance level, displacements greater than 20 cm occur at about 150 m fault distance for concealed or inferred simple traces while they occur at nearly 300 m for inferred or concealed complex traces.

In previous projects, we applied the Petersen et al. (2011) methodology and regression relations to the Hayward fault (Chen et al., 2009) and to the ShakeOut Scenario on the southern San Andreas fault (Chen and Petersen, 2011). These applications incorporated detailed fault traces and produced probabilistic fault displacement hazard maps that are superimposed on the AP Earthquake Fault Zone Maps. As an example, Figure 2 shows a fault displacement hazard map for an area including the Highway 580 and 238 interchange along the Hayward fault. This map shows that the lateral extent of the potential surface fault displacement depends largely on fault complexity and mapping quality. In general, the likelihood of fault displacement decreases as distance from the mapped fault trace increases. The narrowest zone of predicted displacement is along the stretch where the Hayward fault has a single, accurately located trace. Larger width of the zone corresponds to greater fault trace complexity and larger uncertainty in mapped fault trace. Figure 2 suggests that location uncertainty plays an important role, and the treatment of location uncertainty constitutes an essential part of PFDHA. There are two components in location uncertainty: uncertainty associated with the accuracy of existing mapped fault traces (epistemic uncertainty), and natural variability in the location of possible/potential surface rupture around a previously existing, accurately located earthquake fault (aleatory variability). However, in these previous projects we lacked the necessary data to separate these two components of location uncertainty.

Separately quantifying location uncertainty and location variability of surface rupture is the main topic of this project. The uncertainty due to mapping can be removed or reduced by detailed studies using Light Detection and Ranging (LiDAR)-based geographic information system (GIS) analysis, large scale mapping, and/or trenching studies. LiDAR is a laser-based technology with very high positional accuracy and sub-meter resolution, and it is capable of vegetation filtering. Hazard maps, such as Figure 2, can be used to illustrate where detailed fault studies are most valuable to estimate the extent of the area that is subject to significant surface fault displacement. On the other hand, the natural variability associated with rupture location cannot be removed or reduced. However, it can be quantified based on analyses of geological data collected from paleoseismic and other studies. Quantification of natural variability in rupture location enables its explicit inclusion in PFDHA, resulting in better understanding and constraint of estimated fault displacement hazards. It provides a quantitative assessment of the essential part of fault displacement hazard that needs to be incorporated in the design of important lifelines and other structures no matter how much our understanding about the earthquake fault improves. Separate treatment of aleatory variability and epistemic uncertainty in PFDHA also allows an estimate of the amount of design displacement that can be reduced by precise fault location, enabling a risk-informed approach and cost effective measure in design.

This project has three objectives: (1) evaluate data needs for reducing mapping uncertainty (epistemic uncertainty) using published AP fault maps as examples; (2) identify and collect necessary data to quantify natural variability (aleatory variability) in surface fault rupture location; and (3) develop numerical algorithms to treat aleatory variability and epistemic uncertainty separately in PFDHA.

Quantifying surface fault rupture location uncertainty relies on statistical analyses of available data. In this study, we developed three groups of surface fault trace interpretations with varying levels of detail and compared these improved fault locations with AP fault maps to develop necessary data. The first group relies on the recent imagery-based fault studies of Perez et al. (2011) and Treiman et al. (2010). These studies made use of custom-processed sub-meter resolution (0.5 m) LiDAR digital elevation models (DEM), standard aerial photography, and digital multi-spectral imagery. These authors tailored imagery specifically for active fault mapping using an advanced digital image processing technology that integrates MASTER and LiDAR via data fusion to combine their most useful characteristics for fault interpretation. The second and third groups of surface fault interpretations were based entirely on one-meter resolution LiDAR DEMs published by OpenTopography (http://www.opentopography.org/). Compared to the first data group, fault mapping for the second and third data groups is less detailed, but it sampled many major strike-slip faults in California at localities where surface fault features are easily observed and well constrained on LiDAR DEMs.

Location variability data were compiled based on examination of paleoseismic trenches that have identified paleoseismic events, and re-analyses of trench logs from decades of fault investigations for research and development projects in California. This dataset includes 163 trenches located on the following faults (numbers in the parentheses indicate number of trenches examined on each fault): Calaveras (14), Concord (3), Elsinore (7), Fish Lake Valley (1), Hayward (38), Rodgers Creek (8), San Andreas (22), San Jacinto (67), and Simi – Santa Rosa (3).

Fault location uncertainty data were analyzed statistically and our existing PFDHA computer code was modified to account separately for natural variability and mapping uncertainty in rupture location. The modified code follows the standard approach used in the Probabilistic Seismic Hazard Analyses (PSHA) for ground motion hazards for treating epistemic uncertainty and aleatory variability. A simple example is used to illustrate the significance of newly developed data in probabilistic fault displacement estimation.

SURFACE FAULT RUPTURE LOCATION UNCERTAINTY

Traditionally, active faults are mapped by geologists using field methods and aerial photographs or other remote sensing imagery. They record the locations and extents of fault-related geomorphic and stratigraphic features onto a base map. Thus the accuracy of a mapped fault trace depends on quality of the base map, clarity of fault-related features, ability of the geologist to identify these features, availability of reference topography and landmarks, and ability of the geologist to accurately mark the recognized features on the base map.

Maps produced according the National Map Accuracy Standards (http://egsc.usgs.gov/isb/pubs/factsheets/fs17199.html) often include feature location uncertainty specified by the map maker. For example, the USGS 7.5-minute quadrangle topographic maps (standard mapping scale of 1:24,000 or 1 cm equals 240 meters) have an inherent feature location uncertainty of about 15 m. Feature location uncertainty may be larger in certain terrains and for maps produced before modern positioning techniques, such as Global Positioning System (GPS), became available. In addition, features drawn on the base map have uncertainty that is often unknown.

Figure 3 shows the locations where the three groups of epistemic location uncertainty data were collected. The first data group was developed based on extremely detailed mapping of surface faulting-related geomorphic features in two small sections along the southern San Andreas fault near the cities of Indio (about 4 km long) and Yucaipa (about 5-km long) (Treiman et al., 2010), and along a 26-km section in the Antelope Valley near Palmdale (Perez et al., 2011). It is reasonable to assume that all fault branches/splays that have surface expressions in the subject areas are mapped in this group of data. Fault mapping for the second group is less detailed and more selective. The second group of data was sampled from an 82-km section along the southern San Andreas fault in the Carrizo Plain from about 12 km northwest of highway 58 to about 12 km southeast of highway 33, and from a 64-km section long the Garlock fault staring at about 8 km northeast of Koehn Lake. Although the resulting fault maps in this data group may not form a complete set of surface fault traces interpretable from the LiDAR DEMs, all significant traces in the mapped section were carefully examined, especially those that are in the vicinity of previously mapped AP traces. The third data group was mapped specifically for the current project. In developing the third data group, we sampled many strike-slip faults in California that have published LiDAR DEMs, but only at localities where fault-related features are easily identified.

Data Acquisition Methodology

We relied on LiDAR DEMs and other digital imaging techniques to map surface fault ruptures and to demonstrate how location uncertainty associated with previously mapped fault traces can be quantified. In addition to having very high positional accuracy and meter or sub-meter resolution, these digital imaging techniques have the capability to "strip off" vegetation to reveal fault-related features expressed on the ground surface. Faults mapped directly on geographically referenced digital imagery can be recorded directly within the GIS, eliminating inaccuracy introduced by transferring features drawn manually on a base map that is often not geographically referenced. Fault traces based on interpretation of this imagery in GIS are referred to as "interpreted fault traces."

We chose the fault traces of the published AP Earthquake Fault Zone Maps (1:24,000) as previously mapped fault traces and compared them to interpreted fault traces to estimate the uncertainty due solely to mapping inaccuracy. Figure 4 is an example from the Superstition Hills fault showing a 25 – 30 meter discrepancy (*d*) between the mapped trace of the fault (an AP fault trace) compared to a fault scarp shown in the LiDAR-derived hillshade relief image. The mapped fault trace was compiled using traditional methods such as photogrammetry, without the benefit of GPS. The fault scarp shown in this example is a well recognized feature that experienced surface slip or trigger slip from three historical earthquakes: the 1968 M6.6 Borrego Mountain earthquake, the 1979 M6.5 El Centro earthquake, and the 1987 M6.6 Superstition Hills

earthquake. The inaccuracy of the mapped trace, therefore, is due solely to base map resolution and difficulties in transferring a feature that is well recognized in the field to a base map with limited resolution. For faults that do not have historical surface rupture or other easily recognizable surface features, the accuracy of mapped fault location may also be limited by the ability of the geologist to precisely locate the feature in the field. We assessed this uncertainty by comparing the features located on the LiDAR image to the mapped fault traces.

Our sampling strategy focused on associating each mapped fault segment (defined here as an individual line segment drawn by a geologist) with the nearest geomorphic fault feature visible on the LiDAR. This approach operates under the assumption that the feature was originally mapped by the geologist based on the geomorphic expression of the fault, which should also be visible, and perhaps even better expressed, in the LiDAR image. While this uncertainty analysis may not be needed for newer fault maps generated from LiDAR data, uncertainty estimates are important because there are a large number of faults that do not have LiDAR coverage, or that lie outside the relatively narrow (km scale) footprint of LiDAR coverage. Finally, because geologic mapping of active faults typically is compiled at similar scales in other regions and using similar methods, this assessment should be applicable to other regions of the country and perhaps extended in a general way to other types of faulting, where this kind of analysis has not yet been performed.

We developed an efficient approach to sample the interpreted fault traces at a constant interval (25 m) and to measure distances from sample points to various types of previously mapped fault traces (accurately located, approximately located, inferred, and concealed) in the GIS. Figure 5 illustrates sample points (dots) along the interpreted fault traces (green curves) generated using the ArcGIS editing tool, “Densify,” and their association with previously mapped fault traces (identified by color of sample points). The associations were made based on visual inspection of relative location and fault orientation. In Figure 5, red dots are associated with accurately located mapped fault traces (red curves), blue dots are associated with approximately located mapped fault traces (blue long dashed curves), etc. Rupture distance is measured as closest distance from a sample point (dot) to the nearest corresponding (associated) mapped trace using the ArcGIS analysis tool, “Near.” In many cases, imagery-based mapping reveals fault traces that were not mapped previously. These traces are categorized as “previously unmapped” (black dots).

First Group of Location Uncertainty Data

In a research project sponsored by NASA’s Earth Science Applications on Disaster Management, the California Geological Survey (CGS) evaluated the potential of integrated MASTER and high resolution LiDAR data in overcoming inherent limitations of conventional active fault mapping, which is based on aerial photo interpretation and field observations (Perez et al., 2011). MASTER is multispectral imagery with 50 spectral bands ranging from visible to thermal regions of the electromagnetic spectrum. In the Perez et al. (2011) study, MASTER and custom-processed LiDAR were integrated via data transformation/fusion, and the resulting images were utilized to interpret active faults through recognition of fault features associated with different distinctive properties related to geology, drainage, vegetation, hydrology, thermal characteristics, and topography. This study produced much improved and more complete fault interpretations in the 26-km section along the southern San Andreas fault zone, in the Antelope Valley near Palmdale (location is marked by number 1 on Figure 3). Detailed fault

interpretations were made independently by two CGS fault specialists, William Bryant and Jerry Treiman. Figure 6 shows the fault traces interpreted by William Bryant (green), the various categories of previously mapped fault traces using the same color scheme as in Figure 5, and the shaded relief imagery derived from custom-processed, 0.5 m resolution LiDAR DEMs. Table 2 presents summary statistics of fault location uncertainty data. No imagery-based interpreted fault traces were associated with inferred type of previously mapped fault traces. Summary statistics from each fault expert are presented. The last portion of the table presents a summary of overall statistics by weighing the results of the two experts equally.

In research sponsored by the USGS, Treiman et al. (2010) compared the effectiveness of shaded relief imagery derived from high-resolution LiDAR DEMs to standard aerial photography and to digital multi-spectral imagery for identifying and mapping active faults in moderately to sparsely vegetated terrain. This research produced detailed maps of surface faulting-related geomorphic features along the southern San Andreas fault near the cities of Indio (about 4 km long) and Yucaipa (about 5-km long). These two areas have contrasting terrain and vegetation conditions. The Indio area has very little vegetation so that the surface morphology and characteristics are visible in most image types, although some parts have been significantly modified by human activity. The Yucaipa area has more vegetation that masks many of the finer fault features. Faults in this area lie largely within uplifted terrain with greater local relief than the Indio area. Figure 7 shows fault traces (green curves) interpreted based on LiDAR and other imagery in the Indio and Yucaipa study areas. Also shown in this figure are various categories of previously mapped fault traces and shaded relief imagery derived from custom-processed, 0.5 m resolution LiDAR DEMs. Location of the Indio study area is marked by number 2 in Figure 3, and the Yucaipa area by number 3. Table 3 presents basic statistics of fault location uncertainty data. No interpreted fault traces were associated with the inferred type of previously mapped fault traces in this study area.

Second Group of Location Uncertainty Data

Locations for this group of data are identified by numbers 4 (Carrizo Plain) and 5 (Garlock) in Figure 3. The section along the southern San Andreas fault (Carrizo Plain) covers 10 7.5-minute quadrangles of the previously published AP maps, including (from north to south) Las Yeguas Ranch, Simmler, McKittrick Summit, Painted Rock, Panorama Hills, Wells Ranch, Elkhorn Hills, Maricopa, Ballinger Canyon, and Santiago Creek. The section along the Garlock fault covers 8 quadrangles of the previously published AP maps, including (from west to east): Garlock, El Paso Peaks, Klinker Mtn., Cuddeback Lake NW ¼, Spangler Hills East, Searles Lake SE¼, Wingate Pass SW1/4, and Wingate Pass SE¼.

Although, the resulting fault maps in this data group do not represent a complete set of surface fault traces interpretable from the LiDAR images, all significant traces in the mapped section of the southern San Andreas fault were carefully examined, especially those in the vicinity of previously mapped AP traces. Table 4 presents basic statistics of fault location uncertainty data. There are data associated with all four types of previously mapped fault traces in the mapped areas.

Third Group of Location Uncertainty Data

Table 5 lists quadrangle names of previously published AP maps along the various sections of each of the sampled faults in the third data group. Table 6 presents basic statistics of

fault location uncertainty for each fault. This data group shows that San Andreas fault has large location uncertainty compared to other faults sampled in this study, despite being the best known and most thoroughly studied fault. We note that the large location uncertainty in the AP maps reflects the way the AP maps for the San Andreas fault were prepared. They were compiled in 1974 from existing maps without CGS technical review; errors therefore reflect limited air photos and poor quality base maps available before 1974. Later, post 1974, AP maps would be expected to have lower positional errors due to better base maps, more available air photos, and more rigorous CGS review and mapping.

Summary of Location Uncertainty Data Statistics

Table 7 summarizes statistics of data combining all faults from all three data groups. There are a few notable differences between our newly established dataset and our previous fault location uncertainty dataset established based on surface rupture of historical earthquakes (compare Table 7 with Table 1). The new dataset has much smaller scatter for all categories of previously mapped fault traces as shown by smaller standard deviations and COVs. The two datasets have similar mean values for accurately and approximately mapped categories, and the new dataset has smaller mean values compared to the previous dataset for the concealed and inferred categories.

Previously Unmapped Traces

A notable portion of the interpreted fault traces based on LiDAR and other imagery cannot be associated with any previously mapped fault traces (distinctively different location or orientation). These traces are grouped into a new category and are referred to here as "previously unmapped traces." We made an effort to estimate the occurrence probability of these previously unmapped traces only for the 26-km section along the southern San Andreas fault in the Antelope Valley near Palmdale (location marked by number 1 in Figure 3). Imagery-based fault interpretation is comprehensive and complete in this area. The other two areas in the first data group (Indio and Yucaipa) are very small and the data are too sparse to be meaningful. The 2nd and 3rd data groups were not used because LiDAR-based fault interpretation is selective and not complete.

To assess the likelihood of faults that were missed by previous mapping efforts, we followed the methodology of assessing the occurrence of off-fault rupture displacement used in previous studies (Youngs et al., 2003 and Petersen et al., 2011). We digitized regions on both sides of the fault to the maximum extent of previously unmapped fault traces. The probability of finding previously unmapped traces was assessed by calculating the number of cells that contain previously unmapped traces and the total number of cells. Following our previous approach (Petersen et al., 2011) for off-fault rupture, a range of cell sizes from 25 to 200 m was used to better represent the range of areas upon which structures may be built.

Figure 8 illustrates occurrence probability as a function of distance to the nearest previously mapped fault for various cell sizes and for fault interpretations by different fault experts (William Bryant - legends starting with letter B, and Jerry Treiman - legend starting with letter T). Some observations from this figure are as expected. For example, occurrence probability increases with increasing cell size because the larger the cell size the more likely a previously unmapped fault trace is encountered. In general, occurrence probability decreases with increasing fault distance. Interpretations from different experts can be very different,

resulting in very different occurrence probability estimates. This result reflects the challenge of fault mapping, and significant uncertainty exists even with much improved modern imagining technology. It is premature to consider the previously unmapped category in PFDHA because of limited data. However, this exercise illustrates that there is always a probability that some surface faults are left unrecognized and unmapped.

SURFACE RUPTURE LOCATION VARIABILITY

To address the aleatory variability in the location of surface rupture, we quantified width of surface faulting over multiple earthquakes associated with a mapped or primary fault trace. We assess how the width of faulting might vary from earthquake to earthquake. Because few faults have ruptured multiple times historically, and those that have are typically not well-documented in terms of high quality mapping, there is very little observational data regarding the aleatory uncertainty of surface rupture location through time. However, one source of such information is in the geologic record and found in paleoseismic trenching studies, where geologists have trenched across fault zones and have documented the width of faulting and locations of past surface ruptures over multiple seismic cycles. We examined data from paleoseismic trenching studies to ascertain whether or not such studies could shed light on the aleatory variability of surface rupture locations.

Data Availability

In California numerous paleoseismic studies have documented the occurrence of surface faulting in subsurface faulting investigations, typically by digging trenches across fault zones. These studies come in two general varieties. The first type of study is research oriented, aimed at deriving characteristics of fault behavior such as earthquake recurrence and slip rates. These studies are typically published in scientific journals, but also are done sometimes as part of a detailed investigation by a consulting geologist as part of a seismic hazard study, such as for a critical facility (e.g., power plants, dams). The second type of study is usually done in order to identify the locations of faults with the potential to cause surface rupture at a project site. In California, these types of studies are commonly done in order to comply with the AP Act, which stipulates that within Earthquake Fault Zones defined by the State of California, site investigations must be done in order to identify active fault traces and to avoid construction over identified active faults to mitigate surface rupture hazards. For this project, we examined both types of studies, drawing on published scientific investigations as well as studies done for compliance with the AP Act. For the latter, we relied on the CGS database of site investigations, which includes scanned consulting reports, maps, and logs for investigations submitted to CGS as part of the AP Act.

Compilation of Paleoseismic Data

Data were entered into a spreadsheet dataset (Appendix A), which records such attributes as *Fault Name*, *Site Name*, *Site Latitude*, *Site Longitude*, *Mapped Trace Category* (from the AP Zone map), *Trench Number*, and *Comments*. The *Citation* for each site is tagged either by author name and date (for published scientific studies) or indicated as an AP site. Specific types of data we wish to compile are the following data fields:

Trench Length: Length of trench in meters. The length of the trench is recorded because some trenching studies are more extensive than others. Because of this, trench length is important in that there may be a higher probability that a short trench with limited exposure will miss faulting beyond the limits of the trench. Conversely, the longer the trench, the less likely that faulting away from the primary fault is missed.

Maximum Width of Faulting: Maximum width of faulting observed in trench, in meters.

Half Trench Length and *Zone Half Width*: Many trenches are asymmetrically located on one side of the fault, because of natural and man-made obstacles or property lines. This limitation introduces a potential bias when assessing the total width of faulting in that some observations are complete for only one side of the fault zone, while other studies assess the total width of faulting in a more symmetrical way. The "*Half Trench Length*" and "*Zone Half Width*" categories account for this bias by taking the cases where the trench is asymmetrically located across the fault and only measuring the width of faulting on the side with the greatest length of trench. *Half Trench Length* is the length of trench on one side of the fault and *Zone Half Width* is the width of faulting observed for that side. For trenches located more or less symmetrically around the fault, we measure the side of the fault with the most secondary faulting away from the principal or mapped fault.

Event: Number of identified paleoseismic events or a letter or letters designating a particular paleoseismic event in a series of events identified from multiple trenches at the same site.

Event Zone Width: Width of a single event, in meters, measured along the length of the trench.

MRE Trace to Event Distance: For paleoseismic studies with multiple identified events, this measures the distance from the most recent event (MRE) trace (effectively the surface trace) to an earlier event (designated by the *Event* identifier). In cases where there are multiple fault traces, this is taken as the largest distance between traces of the MRE and older event.

Location Variability Data Analysis and Statistics

The location variability dataset includes a total of 163 trenches. Geographic locations of trenches are shown in Figure 3. We analyzed aleatory uncertainty using 3 data fields in Appendix A: zone half width, event zone width, and MRE trace to event distance.

If a particular trench reveals the entire rupture width of an earthquake fault at the trench location, zone half width would be an upper bound of aleatory uncertainty. It is apparent in our dataset (Appendix A) that trench length and revealed rupture zone width are correlated: longer trenches reveal wider rupture zones. However, it is reasonable to assume that zone half width is a good representation of the actual width of the rupture zone on one side of the mapped fault. This is because investigators often dig a trench long enough to reveal the full rupture widths at the trench site and would not stop digging in the middle of an apparent rupture zone. Therefore, in our data analysis, zone half widths from all trenches were used to drive statistics for an upper bound estimate of aleatory location variability without consideration of trench length. The summary statistics are listed in Table 8.

The second parameter that we can infer from the trench data is an approximate lower bound estimate of aleatory location uncertainty. We relied on 53 trenches with identified

paleoseismic events to estimate this parameter. All except one of the trenches with identified paleoseismic events are research trenches. As indicated previously, most researches do not dig trenches wider than necessary to identify all likely paleoseismic events. Based on this understanding, three groups of data are combined: (1) zone half width from 15 trenches with zone half width data and with only one identified event; (2) trench length divided by the number of identified events for the 31 trenches with more than one identified events (i.e., the average distance of an event to the nearest neighboring event); and (3) distance between the most recent event trace to prior event trace. Summary statistics for the lower bound estimate of aleatory location uncertainty are also summarized in Table 8.

Table 8 also provides summary statistics for event zone width. This parameter is not currently factored in the PFDHA methodology. However, it indicates that, on the average, one should expect the surface rupture zone from a single earthquake event to be 1 meter to over 5 meters wide.

Data Limitations

The ability to use paleoseismic data to address the aleatory variability in surface rupture depends on the amount of exposure within a trench both in the lateral sense, away from the primary fault trace, and in a vertical sense, because fault rupture may vary in location from earthquake to earthquake. This variability would be visible only in trenches with stratigraphy that is older than a series of earthquakes. These limitations apply to the paleoseismic data in this compilation in that, collectively, the amount of lateral and vertical trench exposure varies widely from study to study. For the AP type studies, the lateral extent of trench exposure is often limited by the dimensions of the property, or the area a property owner wants “cleared” for a structure. Many studies are limited to a trench that is long enough to encompass the footprint of a building, plus the recommended setback (typically 50 feet from the nearest active fault). In terms of depth, the AP Act requires that buildings be set back from active faults, which are faults that have experienced surface displacement within the past 11,000 years. Because of this requirement, we can generally assume that paleoseismic data compiled for this study have adequate exposure in terms of depth. This observation is particularly true for studies on the most active faults. All of these faults have likely experienced multiple surface rupturing earthquakes during the Holocene. Evidence for faulting can be found in more detailed paleoseismic studies at other locations on the fault, or surface rupturing can be assumed because of a high (>5 mm/yr) slip rate. However, the assumption that AP type studies have adequate depth resolution may be incorrect because many studies, particularly older studies, lack absolute dating control and vary widely in quality. In this study, we did not assess dating controls, nor did we try to assess the quality of the study.

We also found research-level type studies to be problematic because, while most studies are focused on developing long records of earthquakes and have excellent depth resolution, they also tend to be limited in terms of lateral extent. In other words, it appears that once a researcher finds a location amenable to identifying and dating earthquakes, areas away from that trace of the fault receive less attention, making it difficult to have high confidence that the study captures the variability in rupture location at greater distances from the fault.

Finally, we note that this compilation is a limited set of data for strike-slip faults only, compiled to explore the possibility of addressing aleatory variability in fault rupture location. The AP site database and geologic literature may have much more data that could be used to

expand this dataset and make the results much more statistically robust. However, the examination of these records, as we found during the course of this project, is time-consuming and not easily automated, as site investigations need to be reviewed on a case by case basis in order to compile correct data. A parameter that may give a better indication of aleatory location variability is distance from a well identified event to all previous events that are equally well identified. However, that information isn't recorded in any previous trench study. The only way to obtain such measurements is to re-examination all original drawings of trench sections that have multiple well identified paleoseismic events. We also note there are other types of data, such as shallow geophysical data, that may be useful in addressing fault rupture location variability. These types of studies may also provide useful data for future improvements to this compilation.

IMPLEMENTATION OF RUPTURE LOCATION UNCERTAINTY AND VARIABILTY IN PFDHA

In our previous studies (Petersen et al., 2011; Chen and Petersen, 2011), location uncertainty includes both epistemic uncertainty and natural variability, and the uncertainty data were assumed to follow a normal distribution. The probability density function of this normal distribution is integrated in the PFDHA calculation. Here we re-examine the distribution of location uncertainty and variability data obtained from this study, and then explore the ways to implement a probabilistic framework following the standard approaches in PSHA.

The newly acquired data were tested for normality using normal quantile-quantile plots, which relate ranked observations on the vertical axis against the quantile of the normal distribution. A linear relationship suggests that the data come from a normal distribution. The intercept on the vertical axis gives an estimate of the population mean and the slope is an estimate of the standard deviation.

Assuming surface ruptures are equally likely to occur on either side of a mapped fault, the location uncertainty data were randomly assigned a positive or a negative sign to have the uncertainty centered on the mapped fault. Figure 9 shows the normal quantile-quantile plots for the accurately mapped fault trace category for individual faults or fault segments. In general, well sampled faults or fault segments show better normality than poorly sampled ones. Well sampled data include both sets of data along the southern San Andreas fault in the Antelope Valley area, both sets of Garlock data, and data on the southern San Andreas fault near the Carrizo Plain. The normal quantile-quantile plot that combines all accurately mapped data shows that a normal distribution is a good approximation for data within about 2.5 standard deviations (Figure 10). Statistical distribution of all data for the accurately mapped category was further examined by comparing the cumulative data distribution with the theoretical normal cumulative distribution (Figure 11a). Also shown in Figure 11a is an alternative double exponential distribution. Clearly, this dataset follows a normal distribution instead of a double exponential distribution. This result is also demonstrated by the exceedance plots of the two distributions. The data follow the normal exceedace plot (Figure 11b) better than the exponential exceedance plot (Figure 11c).

Figures 12 through 15 show data combining all faults/fault segments plotted against normal and double exponential models for the approximately mapped, concealed, inferred, and previously unmapped categories, respectively. Figure 12 reveals that a normal distribution is not a good approximation for the approximately mapped category data. Instead, the double exponential distribution shows a much better fit. For the concealed category, the data seem to follow normal distribution initially (to approximately 30 m or one standard deviation), then deviate to follow approximately the exponential distribution. In general, the data follow a double exponential distribution better than a normal distribution. The distributions of inferred and previously unmapped categories can be better characterized by double exponential distributions than by normal distributions, although the fit is rather poor.

We modeled the epistemic portion of location uncertainty for the accurately mapped fault trace category with a normal distribution as we had done previously. However, a double exponential distribution seems more appropriate for other categories. Figure 16 compares the probability density for these two distributions. Both distributions are centered on zero (i.e., mapped fault). For a given standard deviation (30 m is used for the curves shown), the overall density charts look similar (Figure 16a). However, on a log-density scale (Figure 16b), exponential is linear and normal is quadratic. This difference means that the likelihood of outliers is different for the two models. If the application is mostly concerned with distances within 1 to 2 standard deviations from the mean (mapped fault), there will be little difference between the two models. However, for distances greater than 2 standard deviations, the two models can give dramatically different results, and the exponential model gives more conservative estimates.

We did not attempt to determine the type of distribution for location variability data because of limited sample size. We continue to assume that location variability is normally distributed.

Implementation in PFDHA

In probabilistic ground motion hazard analyses, it is common to use logic trees to treat epistemic uncertainty. A logic tree consists of a series of branches that describe alternative models/or parameter values. Each branch represents an alternative credible model or parameter. The weights on the branches represent the judgment about the credibility of the alternative models. The branch weights sum to unity. Weights on the branches of logic trees reflect current scientific judgment in the relative merits of the alternative models. Mathematically, weights are probabilities.

We modified our existing PFDHA code to allow a logic tree approach for users to decide whether and how to include location uncertainty. The code provides location uncertainty data from our previous study based on mapped surface ruptures from historical earthquakes and location uncertainty data from imagery-based fault interpretations obtained in this study. These choices result in alternative displacement profiles and hazard curves so that the mean profile and hazard curve can be determined by weighted average, and weights can be selected on a case-by-case basis. Mathematically, both location variability and location uncertainty are accounted for by integrating a probability density function. For variability, we assume a normal distribution. We continue to assume that location uncertainty data from previous historical surface ruptures follow a normal distribution. For the newly acquired data from imagery-based fault

interpretations, however, we adopt a normal distribution for the accurately mapped category and double exponential distributions for other categories.

Example Applications

In this section, we present examples showing how probabilistic estimates of fault rupture hazards may be affected by location uncertainty and variability by examining estimated fault displacement at a given hazard level (10% probability of exceedance in 50 years) along a transect oriented normal to the mapped fault for various location uncertainty and variability cases (Figure 19). In all cases, we modeled a fault that ruptures with a characteristic M7 earthquake on average every 140 years, resulting in a rate of 0.00714 earthquake per year. We performed a probabilistic fault rupture hazard analysis using this single rupture source and did not examine the effects of a Gutenberg–Richter magnitude-frequency distribution. In all calculations, we assumed that the principal fault displacement can occur within 2 standard deviations of the mapped fault trace with standard deviations given in Table 1 for uncertainties obtained previously from historical surface rupture, Table 7 for uncertainties obtained from imagery-based study, and Table 8 for location variability. The uncertainty and variability in terms of standard deviations around the mapped fault are also given in parentheses in Figure 19. In these calculations, we considered the probability of surface rupture on the fault to be one, i.e., we did not allow lack of surface rupture directly along the fault. In addition, probabilistic displacements were calculated using 200 m × 200 m cells and a bilinear regression model and magnitude-distance regression approach discussed in Petersen el al. (2011).

Figure 19 shows the strong effect of different mapping accuracy categories on the estimated displacement. As observed in our previous studies (Petersen et al., 2011; Chen and Petersen, 2011), accurately mapped, approximately mapped, concealed, and inferred fault trace categories have increasingly greater location uncertainty determined from historical surface rupture data (dashed curves in Figure 19). Our calculations indicate that accurately mapped traces have a standard deviation of about 27 m. However, the inferred traces have standard deviations almost three times as large. This higher uncertainty translates into wider displacement profile across the fault and increased hazard at distances beyond 150 m. Similar trends are observed for data from imagery-based analyses. We note that standard deviation from imagery-based analyses is consistently lower than standard deviation determined from historical surface ruptures for a given mapping category, resulting in narrower displacement profile. The fact that COV in imagery-based data is lower than the COV in data from historical surface rupture may indicate lesser degree of variation in the imagery-based dataset.

As expected, displacement profiles (Figure 19) calculated for the two accurately located fault trace category fall between displacement profiles considering only the upper-bound and lower-bound aleatory variability, respectively. This reflects a rather wide range of aleatory variability estimates. If one uses the average of the displacement profiles for the upper and lower bound aleatory estimates, one obtains a displacement profile that is approximately the same as the displacement profiles for the accurately located fault trace category.

DISCUSSION AND CONCLUSIONS

We have demonstrated approaches to develop necessary data to quantify two kinds of location uncertainties in surface fault rupture associated with large earthquakes for probabilistic fault displacement hazard analyses. These are uncertainty associated with the accuracy of existing fault maps (epistemic uncertainty) and natural variability in the location of potential surface rupture around a previously existing, accurately located earthquake fault (aleatory variability).

Quantification of epistemic uncertainty in rupture location is demonstrated using a GIS-based approach and a statistically robust dataset was developed for the published AP Earthquake Fault Zone maps. This dataset and its summary statistics can be utilized directly in engineering practices if a fault displacement hazard analysis is based on the published AP fault maps. AP maps have been widely distributed and routinely referenced in engineering practice in California. One can easily check the availability of these maps and download them from CGS website at: http://www.conservation.ca.gov/cgs/rghm/ap/Pages/Index.aspx. Although the epistemic data and statistics developed in this study apply only to the AP fault maps, the approach is applicable when other fault maps are used. We recommend quantification of epistemic uncertainty for other fault maps if probabilistic fault displacement hazard analyses rely on such maps.

Quantification of aleatory variability in rupture location is challenging because of limited data and many factors affecting the interpretability of available data. We compiled a dataset by examining trenches that have identified paleoseismic events and by re-analyzing trench logs from decades of fault investigations for research and development projects in California. Although the data are not sufficient for establishing a meaningful statistical distribution, we were able to infer an upper bound and a lower bound to aleatory location variability. Our aleatory variability dataset can be applied to strike-slip faults in active tectonic regions similar to California. We note that aleatory variability may be highly dependent on local complexities in the fault, such as changes in strike and stepovers. It may also depend on near surface geologic conditions such as type of soil and surface topography. We also note that some faults may behave in a more predictable manner and produce earthquakes that rupture repeatedly along the same surface fault trace at some locations, such as at the fault scarp shown in Figure 4 along the Superstition Hills fault. We believe that aleatory variability is independent of surface fault trace mapping accuracy (e.g., the fault trace categories in the AP fault maps). However, our aleatory dataset shows larger scatter for concealed and inferred categories. This result may be a manifestation of the effect of near surface fault geometric characteristics on aleatory variability and, subsequently, on a geologist's ability to recognize and accurately map the fault.

We modified our numerical algorithms to treat aleatory variability and epistemic uncertainty separately. A simple example was given to demonstrate that estimated probabilistic fault displacement hazards can be better constrained and are likely reduced if uncertainty due to mapping inaccuracy is removed or reduced. A practical implication of this study is that reducing uncertainty in rupture location can result in more economical design. This benefit may be particularly true for lifelines crossing faults because detailed characteristics of potential displacement profiles (such as those shown in Figure 19) may significantly affect the performance of these lifelines during a surface rupturing earthquake.

ACKNOWLEDGEMENTS

This work was sponsored by the U.S. Geological Survey, National Earthquake Hazards Reduction Program for supporting this study (Award number G11AP20040). We are grateful to William Bryant, Florante Perez, and Jerome Treiman from California Geological Survey for their professional interpretation of LiDAR and other imageries. The authors benefited from insightful discussions with Mark Petersen of U.S. Geological Survey and constructive review comments from Timothy McCrink and William Murphy.

REFERENCES

(This reference list include references cited in Appendix A)

Akciz, S.O., Grant-Ludwig, L., Arrowsmith, J.R., 2009, Revised Dates of Large Earthquakes Along the Carrizo Section of the San Andreas Fault, California Since A.D. 1310 ± 30, *Journal of Geophysical Research*, v 114, doi:10.1029/2007JB005285.

Bryant, W.A., 2012, personal communications.

Buckle, I., Hube, M, Chen, G., Yen, W.H., and Arias, J., 2012, Structural Performances of Bridges in the Offshore Maule Earthquake of 27 February 2010, *Earthquake Spectra*, v 28, n S1, p S179–S197.

Chen, R. and Petersen, M.D., 2011. Mapping Fault Displacement Hazards for the ShakeOut Scenario Using Semi-Probabilistic and Probabilistic Approaches, *Earthquake Spectra*, v 27, n 2, p 293–313.

Chen, R., Wills, C.J., Bryant, W.A., Dawson, T., and Petersen, M.D., 2009, Probabilistic Fault Displacement Hazard on the Hayward Fault Near Hayward, California, *Proceedings of the Third Conference on Earthquake Hazards in the Eastern San Francisco Bay Area: Science, Hazard, Engineering and Risk*, Knudsen K.L. edit., p 129–137.

Dawson, T.E., McGill, S.F., and Rockwell, T.K., 2003, Irregular Recurrence of Paleoearthquakes Along the Central Garlock fault Near El Paso Peaks, California, *Journal of Geophysical Research*, v 108, n B6, p 2823.

Fumal, T.E., Dawson, T.E., Flowers, R., Hamilton, J.C., Heingartner, G.F., Kessler, J., and Samrad, L., 2003a, *Photomosaics and Logs of Trenches on the San Andreas Fault at Mill Canyon near Watsonville, California*, U.S. Geological Survey Open-File Report, 03-469, 1 sheet.

Fumal, T.E., Heingartner, G.F., Samrad, L., Dawson, T.E., Hamilton, J.C., and Baldwin, J.N., 2003b, *Photomosaics and Logs of Trenches on the San Andreas Fault at Arano Flat near Watsonville, California*, U.S. Geological Survey Open-File Report, 03-450, 3 sheets.

Hall, W.J., Nyman, D.J., Johnson, E.R. and Norton, J.D., 2003, Performance of the Trans-Alaska Pipeline in the November 3, 3003 Denali Fault Earthquake, *Proceedings of the Sixth U.S. Conference and Workshop on Lifeline Earthquake Engineering*, ASCE Technical Council on Lifeline Earthquake Engineering, Long Beach, California, August 2003.

Hitchcock, C.S., Lindvall, S.C., Treiman, J.A., Weaver, K.D., Helms, J.G., and Lettis, W.R., 2001, *Paleoseismic Investigation of the Simi Fault, Ventura County, California*, Final Technical Report, USGS NEHRP number 99-HQ-GR-0094.

Kawashima, K., 2002, Damage of Bridges Resulting from Fault Rupture in the 1999 Kocaeli and Duzce, Turkey Earthquakes and the 1999 Chi-Chi, Taiwan Earthquake, *Structural Engineering / Earthquake Engineering*, JSCE., v 19, n 2 [Special Issue], p179s–197s.

Kelson, K.I., Simpson, G.D., Lettis, W.R., and Haraden, C.C., 1996, Holocene Slip Rate and Earthquake Recurrence of the Northern Calaveras Fault at Leyden Creek, Northern California, *Journal of Geophysical Research*, v 101, n B3, p 5961–5975.

Kelson, K.I., Baldwin, J.N., and Randolph, C.E., 1998, *Late Holocene Slip Rate and Amounts of Coseismic Rupture Along the Central Calaveras Fault, San Francisco Bay Area, California*, Technical report to U.S. Geological Survey, National Earthquake Hazards Reduction Program Final Technical Report, Reston, Virginia, under Contract 1434-HQ-97-GR-03151, 26 p.

Kelson, K.I., Koehler, R.D., Baldwin, J.N., Witter, R.C., Lettis, W.R., Sojourner, A.C., 2000, *Paleoearthquake Investigations of the Northern Hayward Fault, San Francisco Bay Region, California*, Final Technical Report, U.S.G.S Award Number 1434-HQ-98-GR-0044, 30p.

Kelson, K.I., Streig, A.R., Koehler, R.D., and Keng-Hao Kang, 2006, Timing of Late Holocene Paleoearthquakes on the Northern San Andreas Fault at the Fort Ross Orchard Site, Sonoma County, California, *Bulletin of the Seismological Society of America*, v 96, p 1012–1028, doi: 10.1785/0120050123.

Lien, Y.W., 1999, *Taiwan Chi-Chi earthquake 9.21.1999 bird's eye view of Cher-Lung-Pu Fault*, Hwang, H.Y. edit, Flying Tiger Cultural, Inc., Taiwan.

Lienkaemper, J.J., and Williams, P.L., 1999, Evidence for Surface Rupture in 1868 on the Hayward Fault in North Oakland and Major Rupturing in Prehistoric Earthquakes: *Geophysical Research Letters*, v 26, n 13, p 1549–1952.

Lienkaemper, J.J., and Williams, P.L., 2007, A Record of Large Earthquakes on the Southern Hayward Fault for the Past 1,800 Years: *Bulletin of the Seismological Society of America*, v 97, n 1, p 803–1,819.

Liu, J., 2008, May 12, *2008 M_S 8.0 Wenchuan Earthquake, Sichuan, China: Background, Field Investigations and Tectonic Implications*, Presentation, the Southern California Earthquake Center 2008 Annual Meeting.

Pamuk, A., Kalkan, E., and Ling H.I., 2005, Structural and Geotechnical Impacts of Surface Rupture on Highway Structures During Recent Earthquakes in Turkey, *Soil Dynamics and Earthquake Engineering*, v 25, issues 7-10, p581–589.

Perez, F.G, Bryant, W.A., Treiman, J.A., Real, C.R., and Hook, S.J., 2011, *Use of Integrated MASTER Multispectral Imagery and LiDAR DEM for Active Fault Detection and Evaluation*, Final Summary of Research, NASA Grant NNX09AP59G.

Petersen, M.D., Dawson, T.E., Chen, R., Cao, T., Wills, C.J., Schwartz, D.P., and Frankel, A.D., 2011, Fault Displacement Hazard for Strike-Slip Faults. *Bulletin of the Seismological Society of America*, v 101, n 2, p 805–825.

Reheis, M.C., 1994, *Logs of Trenches Across the Central Part of the Fish Lake Valley Fault Zone, Mono County, California*, U.S. Geological Survey MF-2266, 20 p, 1 sheet.

Rockwell, T.K., McElwain, R.S., Millman, D.E., and Lamar, D.L., 1986, Recurrent Late Holocene Faulting on the Glen Ivy North Strand of the Elsinore Fault at Glen Ivy Marsh, in Ehlig, P.L., ed., *Neotectonics and Faulting in Southern California: Geological Society of America*, 82nd Annual Meeting of the Cordilleran Section, Guidebook and Volume, p. 167–175.

Rockwell, T.K., Seitz, G.G., Young, J., and Dawson, T.E., 2004, *Late Holocene Earthquake History of the Anza Seismic Gap Central San Jacinto Fault Zone, Southern California*, USGS Final Technical Report, 13p.

Rubin, C.M., and Sieh, K., 1997, Long Dormancy, Low Slip Rate, and Similar Slip-Per-Event for the Emerson Fault, Eastern California Shear Zone, *Journal of Geophysical Research*, v 102, p 15319–15333.

Shlemon, R.J., 2010, A Proposed Mid-Holocene Age Definition for Hazardous Faulting in California: *Environmental and Engineering Geosciences*, v 16, n 1, p 55–64.

Simpson, G.D., Baldwin, J.N., Kelson, K.I., and Lettis, W.R., 1999, Late Holocene Slip Rate and Earthquake History for the Northern Calaveras Fault at Welch Creek, Eastern San Francisco Bay Area, California, *Bulletin of the Seismological Society of America*, v 89, p 1250–1263.

Treiman, J.A., Perez, F.G., and Bryant, W.A., 2010, *Utility of Combined Aerial Photography and Digital Imagery for Fault Trace Mapping in Diverse Terrain and Vegetation Regimes*, Final Technical Report, USGA Award No. 08HQGR0096.

Vaughan, P.R., Thorup, K.M., and Rockwell, T.K., 1999, Paleoseismology of the Elsinore Fault at Agua Tibia Mountain, *Bulletin of the Seismological Society of America*, v 89, p 1447–1457.

Wong, P., Bryant, W.A., and Treiman, J.A., 2003, *Fault Investigation Reports for Development within Alquist-Priolo Earthquake Fault Zones in Northern California*, 1974–2000, California Geological Survey CD 2003-01.

Wong, P., Bryant, W.A., and Treiman, J.A., 2003, *Fault Investigation Reports for Development within Alquist-Priolo Earthquake Fault Zones in Southern California*, 1974–2000, California Geological Survey CD 2003-02.

Xu, X., Wen, X., Ye, J., Ma, B., Chen, J., Zhou, R., He, H., Tian, Q., He, Y., Wang, Z., Sun, Z., Feng, X., Yu, G., Chen, L., Chen, G., Yu, S., Ran, Y., Li, C., and An, Y., 2008, The Ms 8.0 Wenchuan Earthquake Surface Ruptures and Its Seismogenic Structure, *Seismology and Geology*, v 30, p 597–629 (in Chinese).

Youngs, R.R., Arabasz, W.J., Anderson, R.E., Ramelli, A.R., Ake, J.P., Slemmons, D.B., McCalpin, J.P., Doser, D.I., Fridrich, C.J., Swan III, F.H., Rogers, A.M., Yount, J.C., Anderson, L.W., Smith, K.D., Bruhn, R.L., Knuepfer, L.K., Smith, R.B., dePolo, C.M., O'Leary, K.W., Coppersmith, K.J., Pezzopane, S.K., Schwartz, D.P., Whitney, J.W., Olig, S.S., and Toro, G.R., 2003, A Methodology for Probabilistic Fault Displacement Hazard Analysis (PFDHA), *Earthquake Spectra*, v 19, n1, p 191–219.

TABLES AND FIGURES

Table 1. Summary statistics for location uncertainty determined by Petersen et al. (2011) based on surface ruptures from historic earthquakes

Type of Mapped Trace	mean (m)	one-sided σ	COV	two-sided σ
Accurate	18.5	19.5	1.1	26.9
Approximate	25.2	35.9	1.4	43.8
Concealed	39.4	52.4	1.3	65.5
Inferred	45.1	57.0	1.3	72.7
All	30.6	43.1	1.4	52.9

Table 2. Summary statistics of fault location uncertainty for data group 1 (Antelope area)

Fault traces in Antelope mapped by William Bryant				
Type of Mapped Trace	Mean (m)	One-Sided σ	Two-Sided σ	Number of Points
Accurate	10.6	8.2	13.5	1053
Approximate	19.0	20.9	28.2	2018
Concealed	40.4	31.6	51.3	298
Inferred	-	-	-	-
All-Data	18.3	20.8	27.7	3369
All-Type	23.3	20.2	30.9	3
Unmapped	172.3	170.5	45.1	573
Fault traces in Antelope mapped by Jerry Treiman				
	Mean (m)	One-Sided σ	Two-Sided σ	Number of Points
Accurate	13.5	10.9	17.3	1590
Approximate	26.6	25.9	37.1	3142
Concealed	39.9	30.3	50.1	557
Inferred	-	-	-	-
All-Data	24.0	24.4	34.2	5289
All-Type	26.7	22.3	34.8	3
Unmapped	190.8	139.2	236.1	2916
Statistics for Fault Traces in Antelope (average of Bryant and Treiman)				
	Mean (m)	One-Sided σ	Two-Sided σ	-
Accurate	12.1	9.6	15.4	-
Approximate	22.8	23.4	32.6	-
Concealed	40.2	30.9	50.7	-
Inferred	-	-	-	-
All-Data	21.2	22.6	30.9	-
All-Type	25.0	21.3	32.8	-
Unmapped	181.5	154.8	238.6	-

Table 3. Summary statistics of fault location uncertainty for data group 1 (Indio and Yucaipa areas)

Fault traces in the Indio Study Area				
Type of Mapped Trace	Mean (m)	One-Sided σ	Two-Sided σ	Number of Points
Accurate	20.8	18.6	27.9	503
Approximate	65.3	42.1	77.7	68
Concealed	-	-	-	-
Inferred	-	-	-	-
All-Data	26.1	26.9	37.5	571
All-Type	43.0	30.4	52.7	2
Unmapped	131.5	68.7	45.1	53
Fault traces in Yucaipa Study Area				
Type of Mapped Trace	Mean (m)	One-Sided σ	Two-Sided σ	Number of Points
Accurate	16.1	12.0	20.0	186
Approximate	18.7	18.3	26.2	444
Concealed	23.0	18.5	29.5	114
Inferred	-	-	-	-
All-Data	18.7	17.1	25.3	744
All-Type	19.2	16.3	25.2	3
Unmapped	80.1	39.4	89.3	83

Table 4. Summary statistics of fault location uncertainty for data group 2

Southern San Andreas Fault - Carrizo Plain				
Type of Mapped Trace	Mean (m)	One-Sided σ	Two-Sided σ	Number of Points
Accurate	18.5	12.9	22.6	4654
Approximate	29.6	26.6	39.9	2368
Concealed	28.1	22.8	36.2	31
Inferred	72.2	53.8	90.1	182
All-Data	23.5	22.4	32.5	7235
All-Type	37.1	29.0	47.1	4
Unmapped	186.6	153.2	45.1	1681
Garlock Fault - Central and East				
Type of Mapped Trace	Mean (m)	One-Sided σ	Two-Sided σ	Number of Points
Accurate	13.9	11.9	18.3	4345
Approximate	31.1	24.4	39.6	725
Concealed	21.6	15.1	26.3	350
Inferred	17.7	12.5	21.7	521
All-Data	16.8	15.3	22.8	5941
All-Type	21.1	16.0	26.5	4
Unmapped	147.7	216.2	261.9	1838

Table 5. Quadrangles of the previously published AP maps along sections of faults sampled in data group 3

Southern San Andreas Fault	
Holland Canyon	Elkhorn Hills
La Panza NE	Maricopa
Las Yeguas Ranch	LaLiebre Ranch
McKittrick Summit	Telegraph Peak
Painted Rock	San Bernardino North
Panorama Hills	Morongo Valley SE1/4
Well Ranch	
Northern San Andreas Fault	
Point Arena	Cherry Peak
Fort Ross	Bickmore Canyon
Montara Mountain	San Benito
Mindego Hill,	Topo Valley
Castle Rock Ridge	Rock Spring Peak
Paicine	
Hayward-Rodgers Creek Fault	
Healdsburg	Sears Point
Cotati	Lick Observatory
Glen Ellen	
San Jacinto Fault	
Brawley NW	Clark Lake NE
Fonts Point	
Elsinore	
Arroyo Taplado	Earthquake Valley
Monument Peak	
Garlock	
Mojave NE1/4	Wingate Pass SE
Klinker Mtn	Quail Mountains SW
Spangler Hills East	Quail Mountains SE
Searles Lake SE	Leach Lake SW
Wingate Pass SW	Leach Lake SE
Ash Hill Fault	
Maturango Peak SE	Revenue Canyon
Maturango Peak NE	Panamint Springs
Lenwood Fault	
Old Woman Springs	Grand View Mine
Fry Mountains	
Panamint Fault	
Hidden Spring	Manly Fall
Copper Queen Canyon	Wingate Pass
Sourdough Spring	Quail Mountains SW1

Table 6. Summary statistics of fault location uncertainty for data group 3

Southern San Andreas Fault				
Type of Mapped Trace	Mean (m)	One-Sided σ	Two-Sided σ	Number of Points
Accurate	25.4	15.2	29.6	1734
Approximate	55.0	34.0	64.6	137
Concealed	31.4	2.8	31.5	11
Inferred	-	-	-	-
All-Data	27.6	18.9	33.4	1882
All-Type	37.3	17.3	41.1	3
Unmapped	483.7	209.8	527.3	149
Northern San Andreas Fault				
Type of Mapped Trace	Mean (m)	One-Sided σ	Two-Sided σ	Number of Points
Accurate	28.2	19.8	34.4	678
Approximate	17.1	14.3	22.3	65
Concealed	42.5	17.6	46.0	30
Inferred	-	-	-	-
All-Data	27.8	19.8	34.1	773
All-Type	29.3	17.2	34.0	3
Unmapped	-	-	-	-
Hayward-Rodgers Creek Fault				
Type of Mapped Trace	Mean (m)	One-Sided σ	Two-Sided σ	Number of Points
Accurate	21.6	16.2	27.0	155
Approximate	34.4	24.3	42.1	110
Concealed	76.2	9.8	76.9	6
Inferred	21.1	18.1	27.8	48
All-Data	27.0	21.5	34.5	319
All-Type	44.1	16.8	47.2	3
Unmapped	198.9	17.7	199.7	50
San Jacinto Fault				
Type of Mapped Trace	Mean (m)	One-Sided σ	Two-Sided σ	Number of Points
Accurate	19.2	12.4	22.9	311
Approximate	-	-	-	-
Concealed	24.4	11.3	26.9	39
Inferred	-	-	-	-
All-Data	19.8	12.4	23.4	350
All-Type	21.8	11.9	24.8	2
Unmapped	81.3	32.7	87.6	33

Table 6. Summary statistics of fault location uncertainty for data group 3 (cont.)

Elsinore Fault				
Type of Mapped Trace	Mean (m)	One-Sided σ	Two-Sided σ	Number of Points
Accurate	16.0	15.0	21.9	203
Approximate	-	-	-	-
Concealed	-	-	-	-
Inferred	-	-	-	-
All-Data	16.0	15.0	21.9	203
All-Type	16.0	15.0	21.9	1
Unmapped	51.3	37.2	63.4	97
Garlock Fault				
Type of Mapped Trace	Mean (m)	One-Sided σ	Two-Sided σ	Number of Points
Accurate	20.5	14.2	24.9	1781
Approximate	36.5	18.7	41.0	124
Concealed	27.2	13.7	30.5	54
Inferred	29.8	27.7	40.7	144
All-Data	22.2	16.3	27.6	2103
All-Type	28.5	18.6	34.0	4
Unmapped	116.9	159.7	197.9	388
Ash Hill Fault				
Type of Mapped Trace	Mean (m)	One-Sided σ	Two-Sided σ	Number of Points
Accurate	18.5	12.3	22.2	245
Approximate	16.4	14.5	21.9	354
Concealed	43.6	34.4	55.5	99
Inferred	-	-	-	-
All-Data	21.0	20.3	29.2	698
All-Type	26.1	20.4	33.2	3
Unmapped	368.1	510.5	629.3	629
Lenwood Fault				
Type of Mapped Trace	Mean (m)	One-Sided σ	Two-Sided σ	Number of Points
Accurate	19.7	15.4	25.0	179
Approximate	20.3	18.6	27.5	139
Concealed	40.0	7.4	40.7	22
Inferred	16.8	13.5	-	68
All-Data	20.5	16.7	26.5	406
All-Type	24.2	13.7	27.8	4
Unmapped	216.3	71.9	228.0	39

Table 6. Summary statistics of fault location uncertainty for data group 3 (cont.)

Panamint Fault				
Type of Mapped Trace	Mean (m)	One-Sided σ	Two-Sided σ	Number of Points
Accurate	9.8	7.6	12.4	400
Approximate	17.6	14.2	22.6	377
Concealed	21.7	14.5	26.1	58
Inferred	27.1	18.5	32.8	69
All-Data	15.1	13.3	20.1	904
All-Type	19.1	13.7	23.5	4
Unmapped	77.7	71.0	105.3	43

Table 7. Summary statistics of data combining all faults of all three data groups

Type of Mapped Trace	Mean (m)	One-Sided σ	COV	Two-Sided σ	Number of Points
Accurate	17.7	13.9	0.8	22.5	17951
Approximate	25.8	25.0	1.0	35.9	10071
Concealed	33.9	27.3	0.8	43.5	1675
Inferred	29.8	33.9	1.1	45.1	1030
All	21.6	20.5	0.9	29.8	31038
Unmapped	190.4	221.8	1.2	292.3	8572

Table 8. Summary statistics of location variability data

Representation	Mean (m)	One-Sided σ	COV	Two-Sided σ	Number of Data Points
Upper Bound	17.4	32.3	1.85	36.7	125
Lower Bound	10.0	10.1	1.01	14.2	52
Event zone width	2.8	2.6	0.93	3.9	49

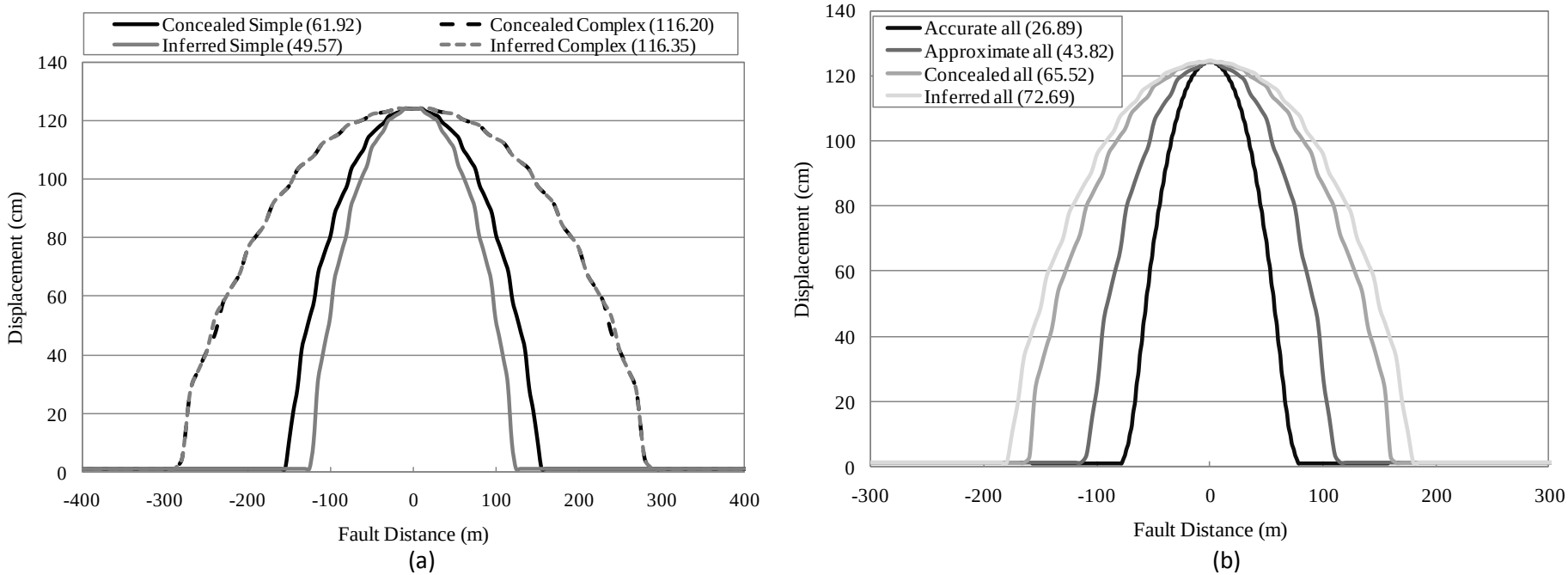

Figure 1. Examples of calculated displacement hazard profiles showing displacements across a mapped fault for a hazard level of 10% probability of exceedance in 50 years for: (a) different mapping quality, (b) different complexity characteristics (Petersen et al., 2010). The examples are for a M7.0 earthquake occurring once every 140 years.

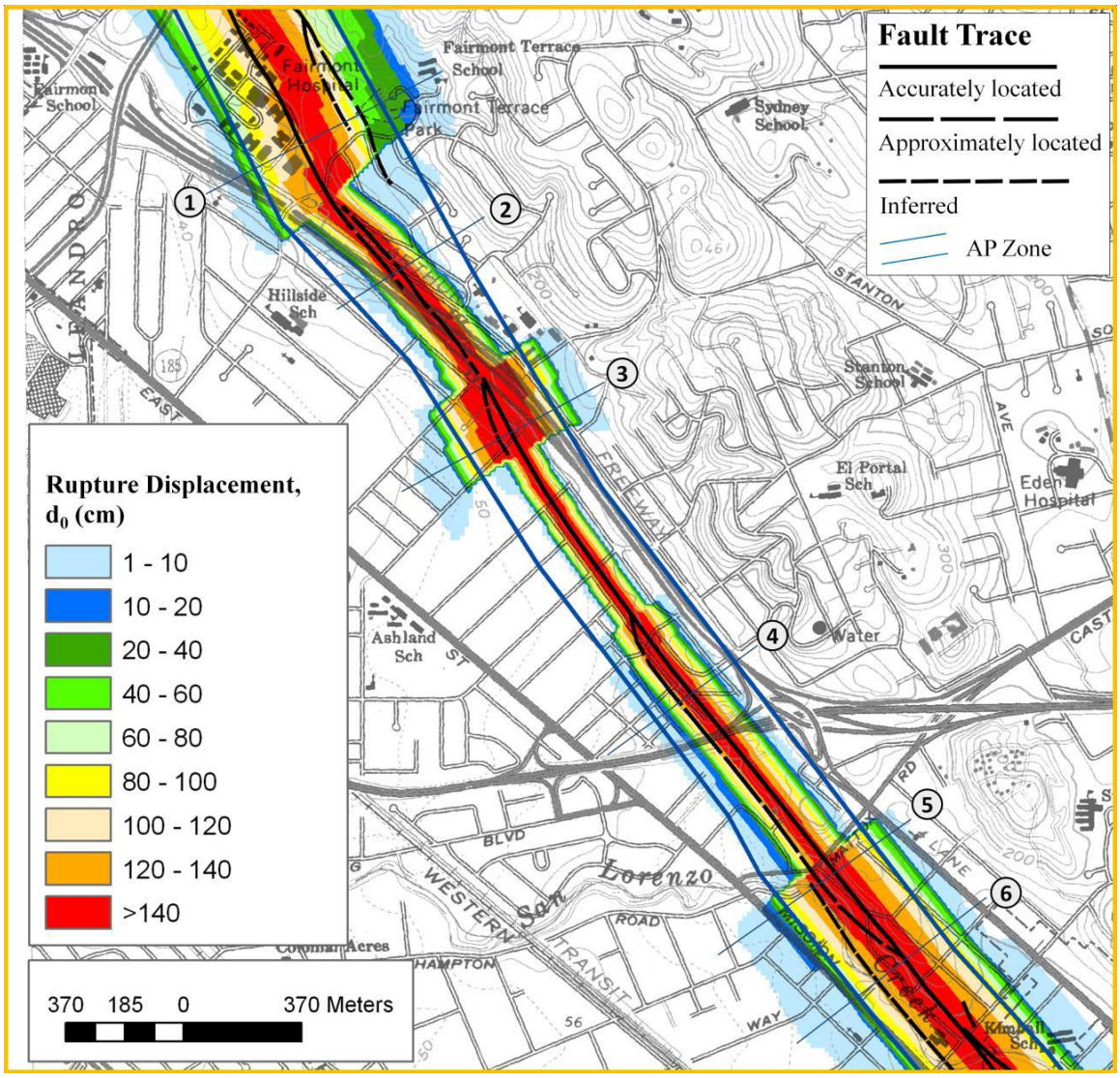

Figure 2. Example of probabilistic fault displacement hazard map with 10% probability of being exceeded in 50 years at the Highway 580-238 interchange (Chen et al., 2009).

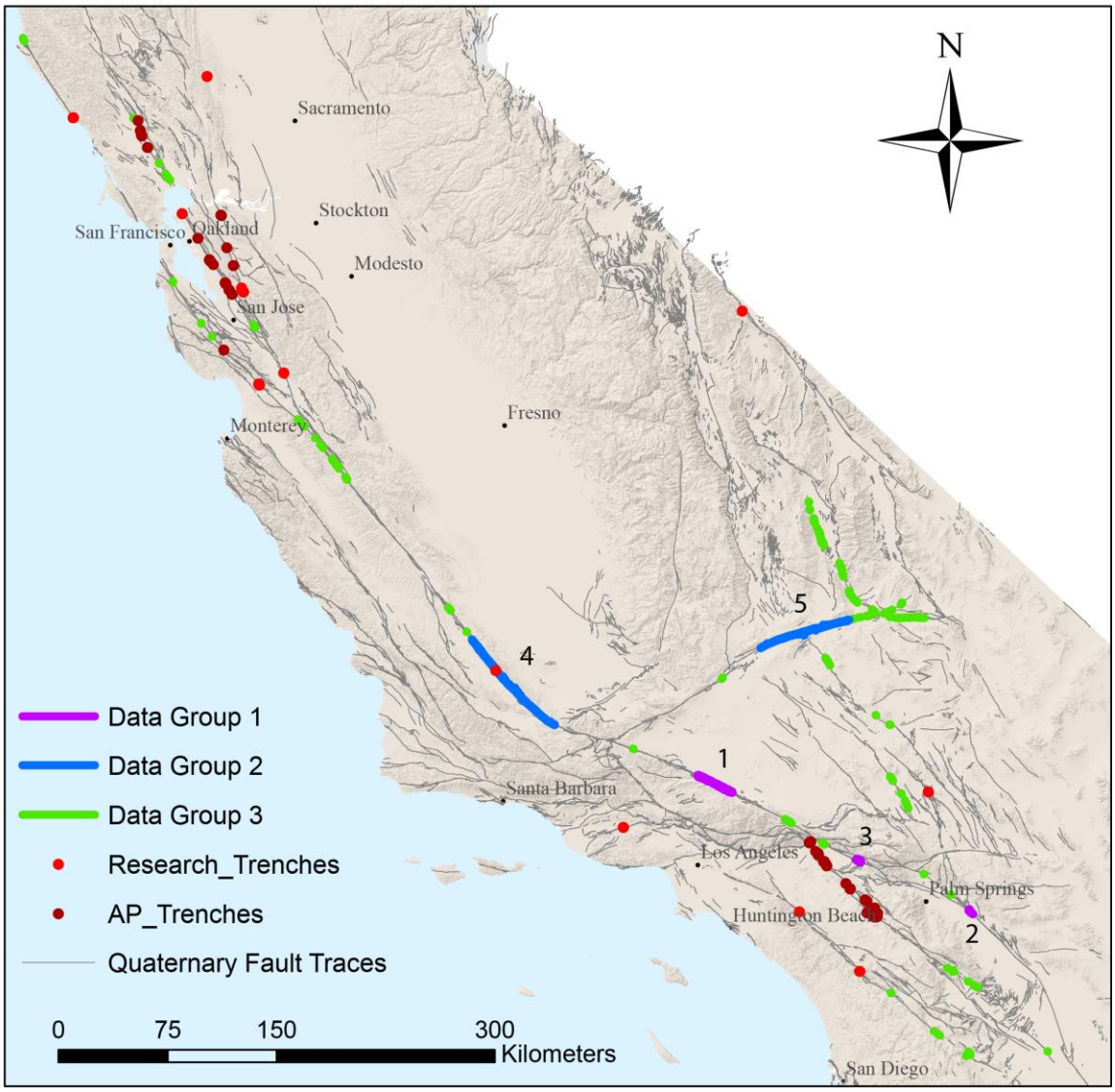

Figure 3. Locations of three groups of surface fault location uncertainty data sites (1 – Antelope, 2 – Indio, 3 – Yucaipa, 4 – Carrizo Plain, and 5 – Garlock) and trenches studied for fault location variability data.

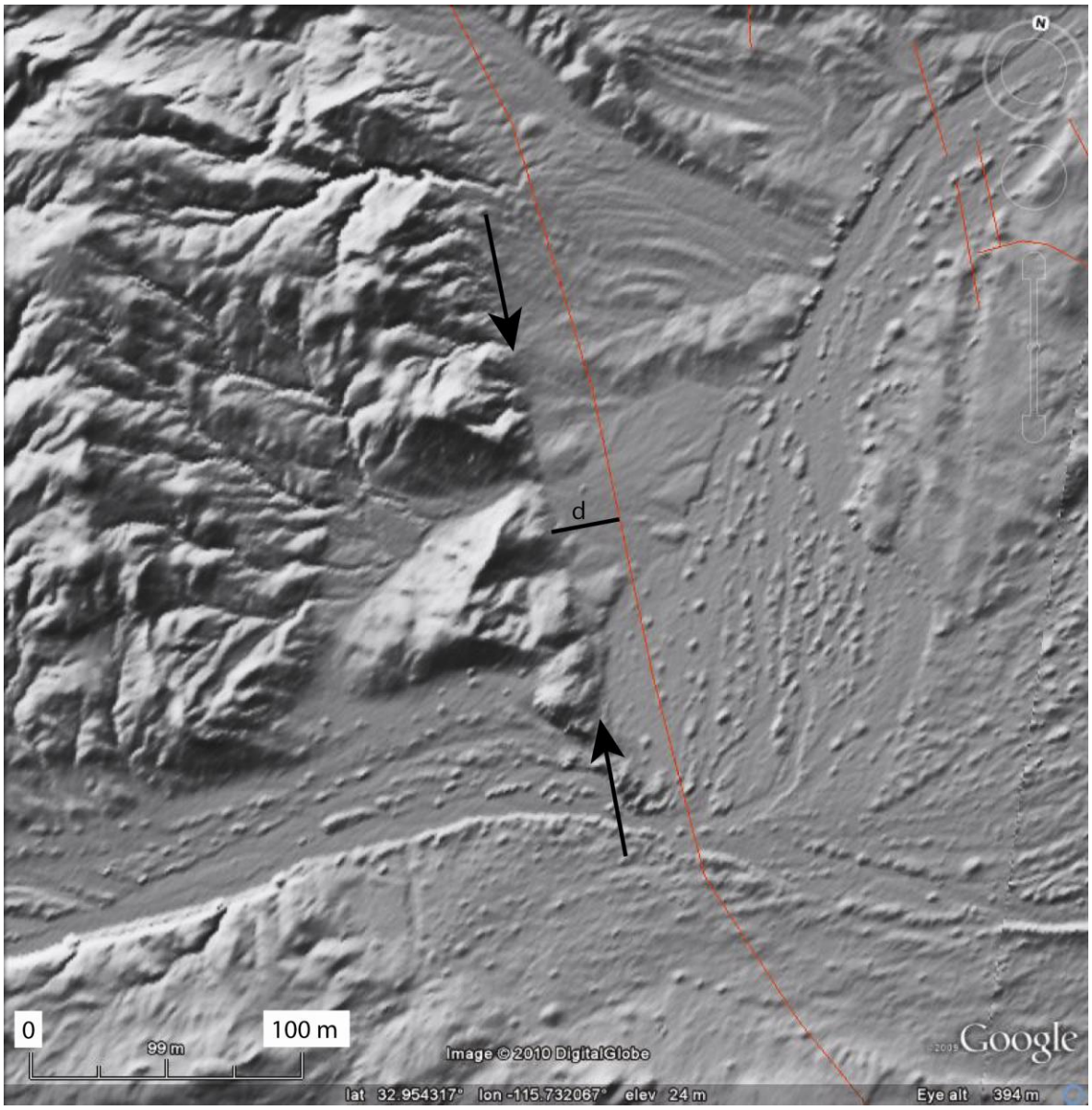

Figure 4. LiDAR hillshade relief map showing the relation between location of fault scarp (shown by arrows) and mapped fault trace locations (in red) taken from a 1:24,000-scale Alquist-Priolo Earthquake Fault Zone map. In this case, the discrepancy between the mapped fault trace and the geomorphic fault feature, labeled "d", is about 30 m. The high horizontal accuracy of the LiDAR (sub-meter) allows direct comparison between the mapped fault location and the location of the fault-related feature on the Earth's surface. This discrepancy is associated with the epistemic uncertainty in the 1:24,000 scale mapping.

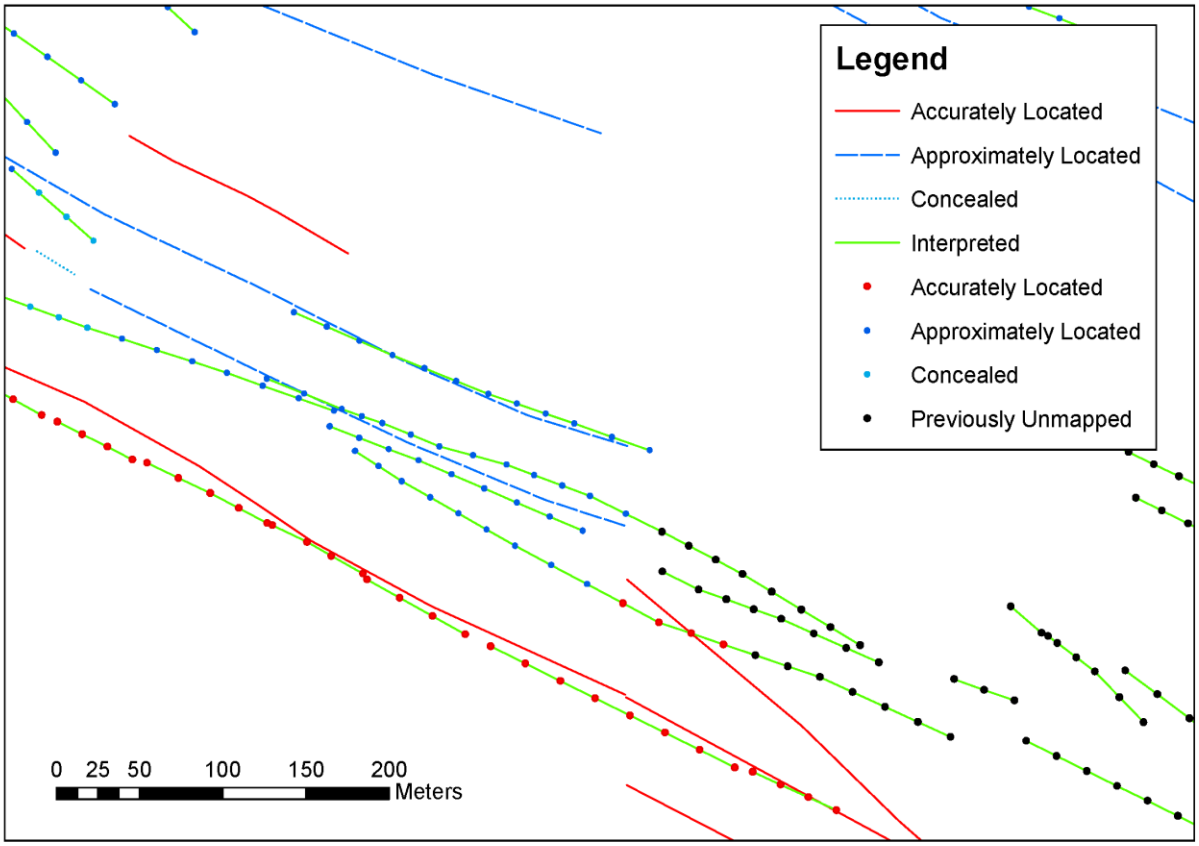

Figure 5. Comparison of fault features interpreted based on LiDAR and other imagery with fault traces previously mapped in the Alquist-Priolo Earthquake Fault Zone Maps, illustrating equal interval sample points along the interpreted fault features and their association with the mapped fault traces. Distances from sample points to the nearest mapped fault traces are measured and analyzed.

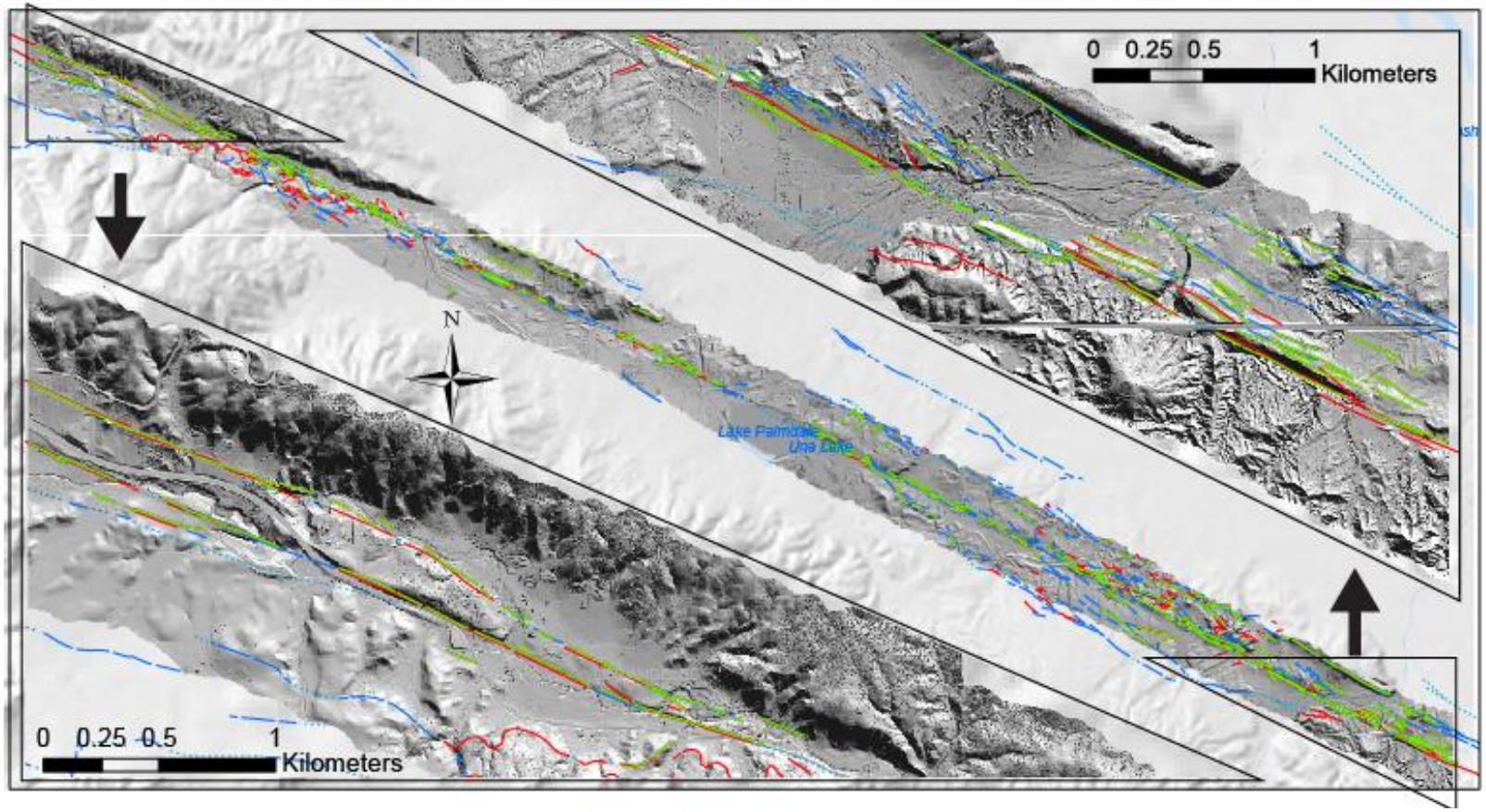

Figure 6. Fault traces (green) interpreted based on LiDAR and other imagery from Perez et al. (2011). Also shown are various categories of previously mapped fault traces (accurately located, approximately located, concealed, and inferred; see Figure 5 legends for color scheme) and custom-processed LiDAR DEMs. For reference, location of this segment of the San Andreas fault is marked by number 1 in Figure 3.

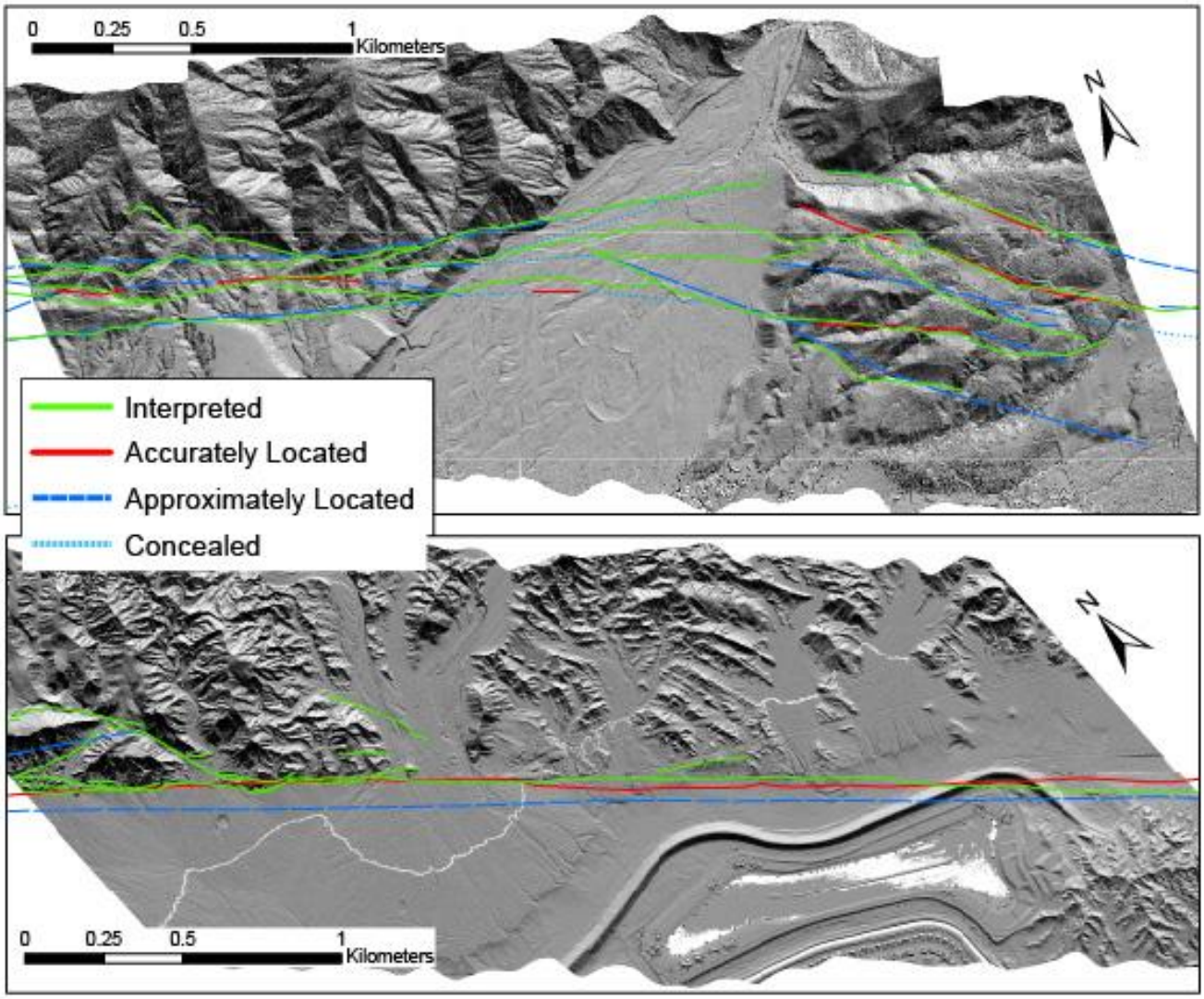

Figure 7. Fault traces (green) interpreted based on LiDAR and other imagery from Treiman et al. (2010) in the Yucaipa (upper figure) and Indio (lower figure) study areas along the southern San Andreas fault. Also shown are various categories of previously mapped fault traces and custom-processed LiDAR DEMs. For reference, location of the Indio study area is marked by number 2 in Figure 3, and the Yucaipa area by number 3.

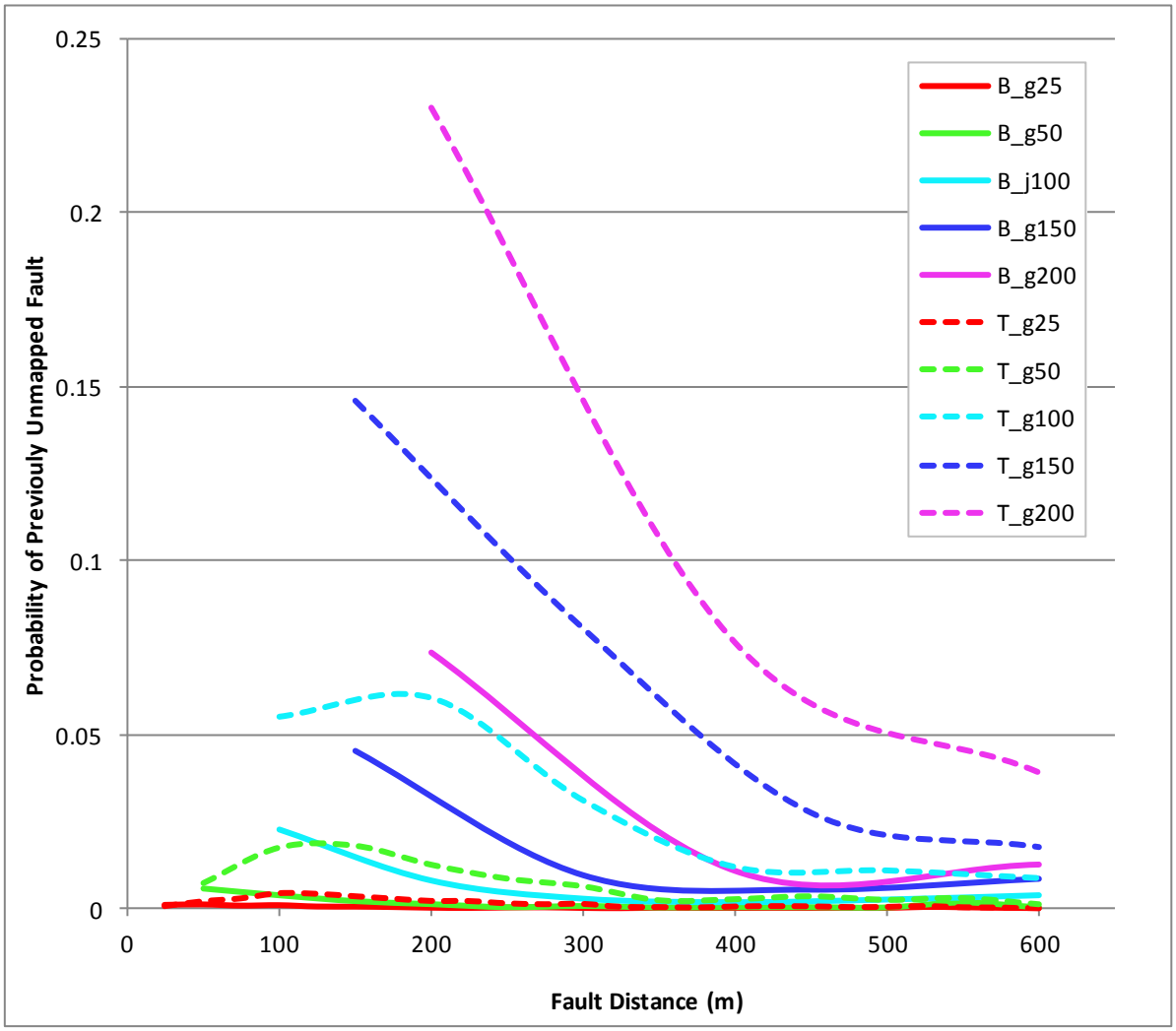

Figure 8. Existence Probability of previously unmapped traces from imagery-based fault interpretation by two CGS fault experts, William Bryant (legends starting with letter B) and Jerry Trainmen (legend starting with letter T), in a 26-km section along the southern San Andreas fault in the Antelope Valley near Palmdale (location marked by number 1 on Figure 3). The probability assessments were based on square grids of cell sizes of 25 m^2, 50 m^2, 100 m^2, 150 m^2, and 200 m^2, respectively.

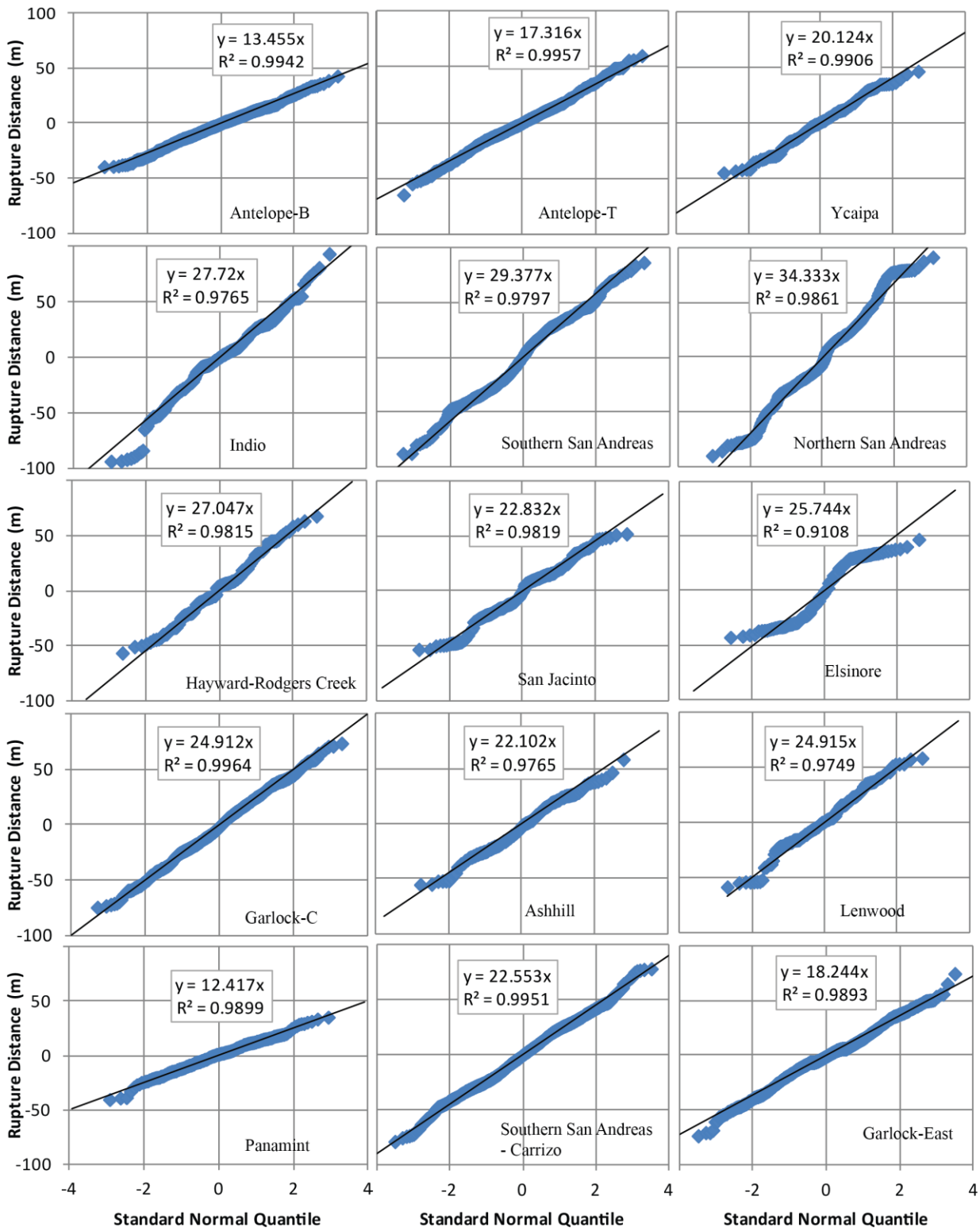

Figure 9. Normal quantile-quantile plot. A normal quantile-quantile plot plots the ranked observations on the vertical axis against the quantile of the normal distribution. A nearly straight-line relationship suggests that the data come from a normal distribution. The intercept on the vertical axis is an estimate of the population mean, μ, and the slope is an estimate of the standard deviation, σ.

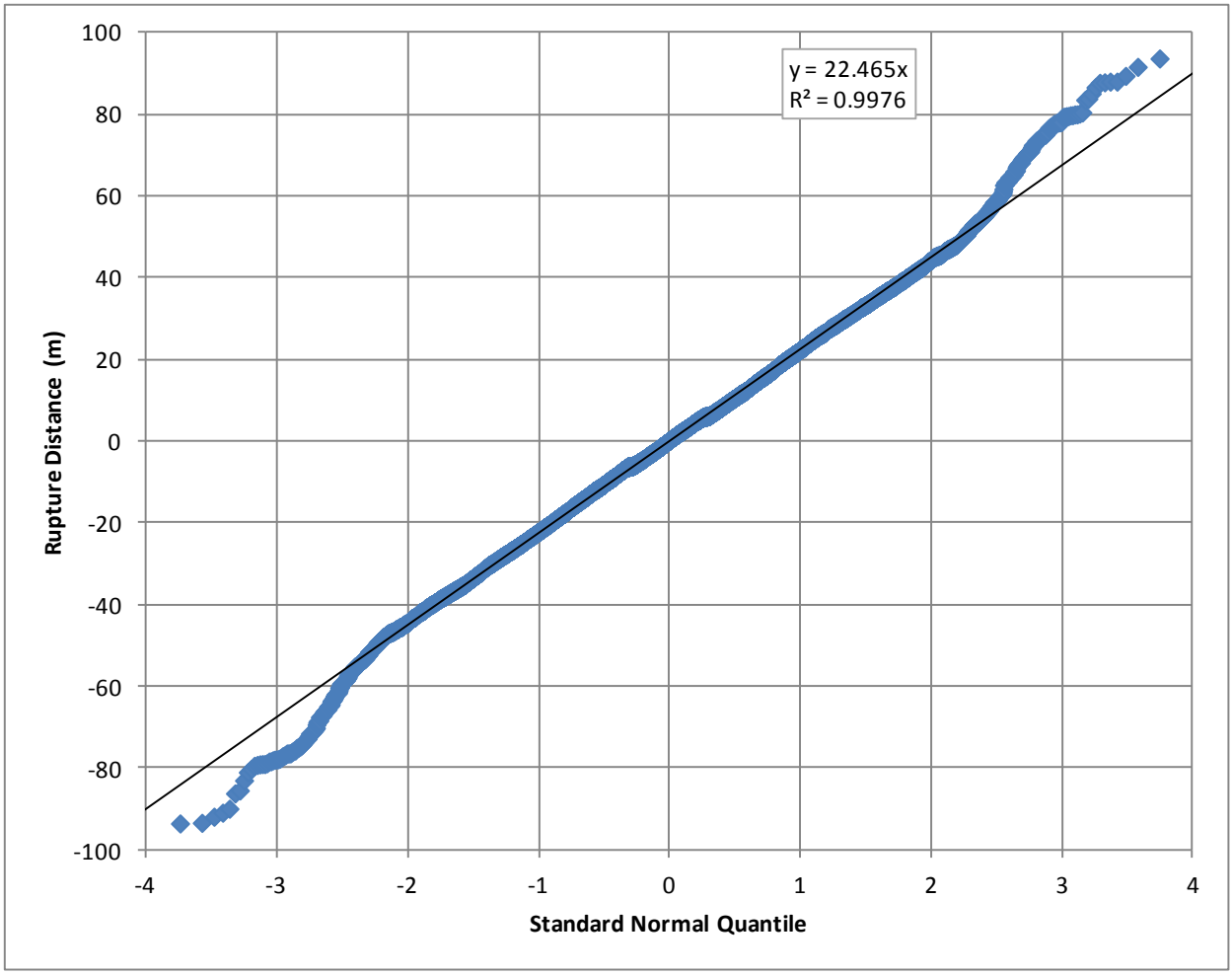

Figure 10. Normal quantile-quantile plot combining all of the accurately mapped fault data. It shows that the normal distribution is a good approximation for data within 2.5 standard deviations. When centered on the mapped fault (zero intercept), the slope of the least-squares best-fit line is 22.5 m. This slope is the same as the two-sided sample standard deviation for all accurately mapped data.

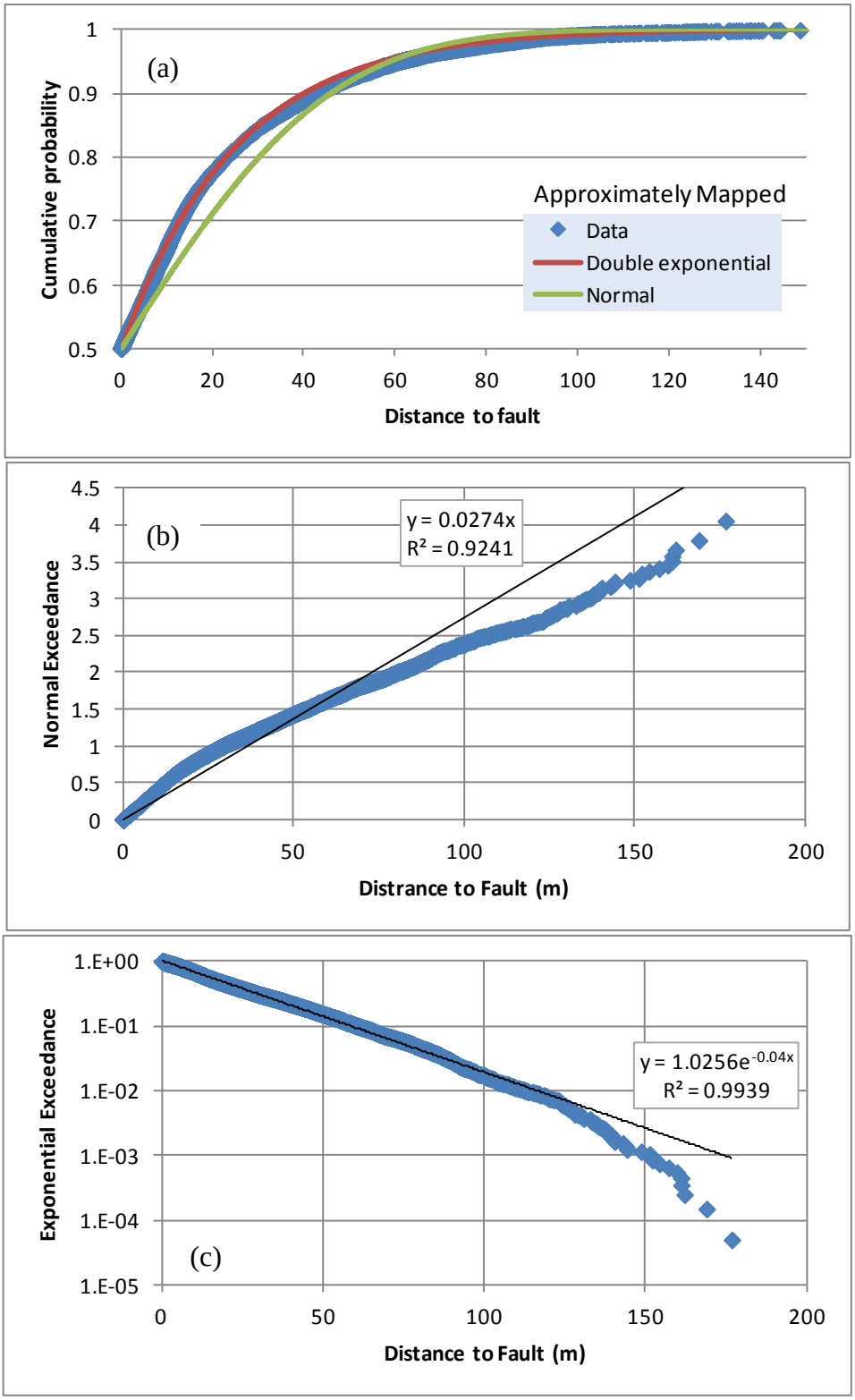

Figure 12. Comparison of approximately mapped fault distance data combining all faults/fault segments: a. data cumulative distribution compared to theoretical normal and exponential cumulative distributions; b. exceedance plot for normal distribution; c. exceedance plot for exponential distribution.

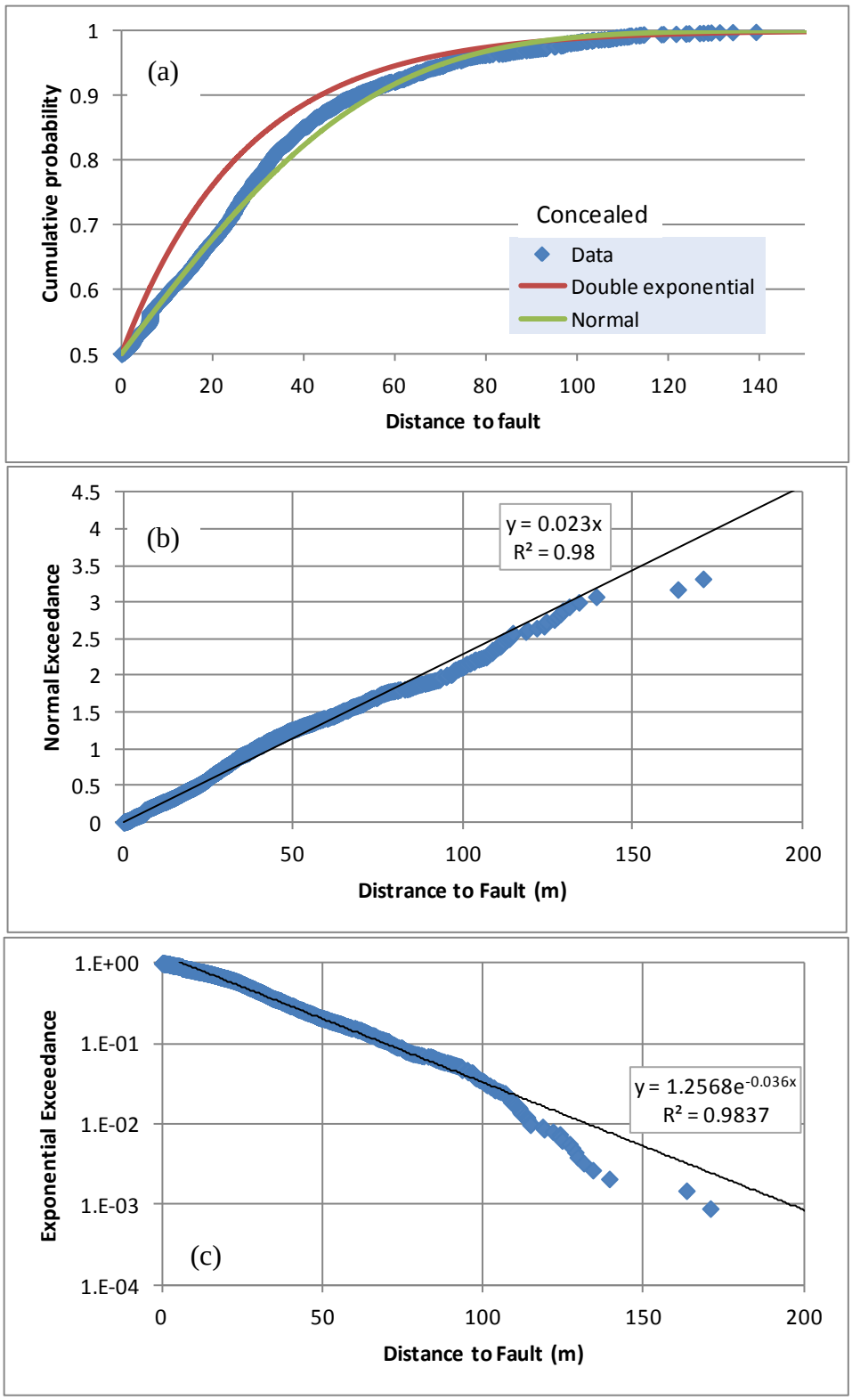

Figure 13. Comparison of concealed fault distance data combining all faults/fault segments: a. data cumulative distribution compared to theoretical normal and exponential cumulative distributions; b. exceedance plot for normal distribution; c. exceedance plot for exponential distribution.

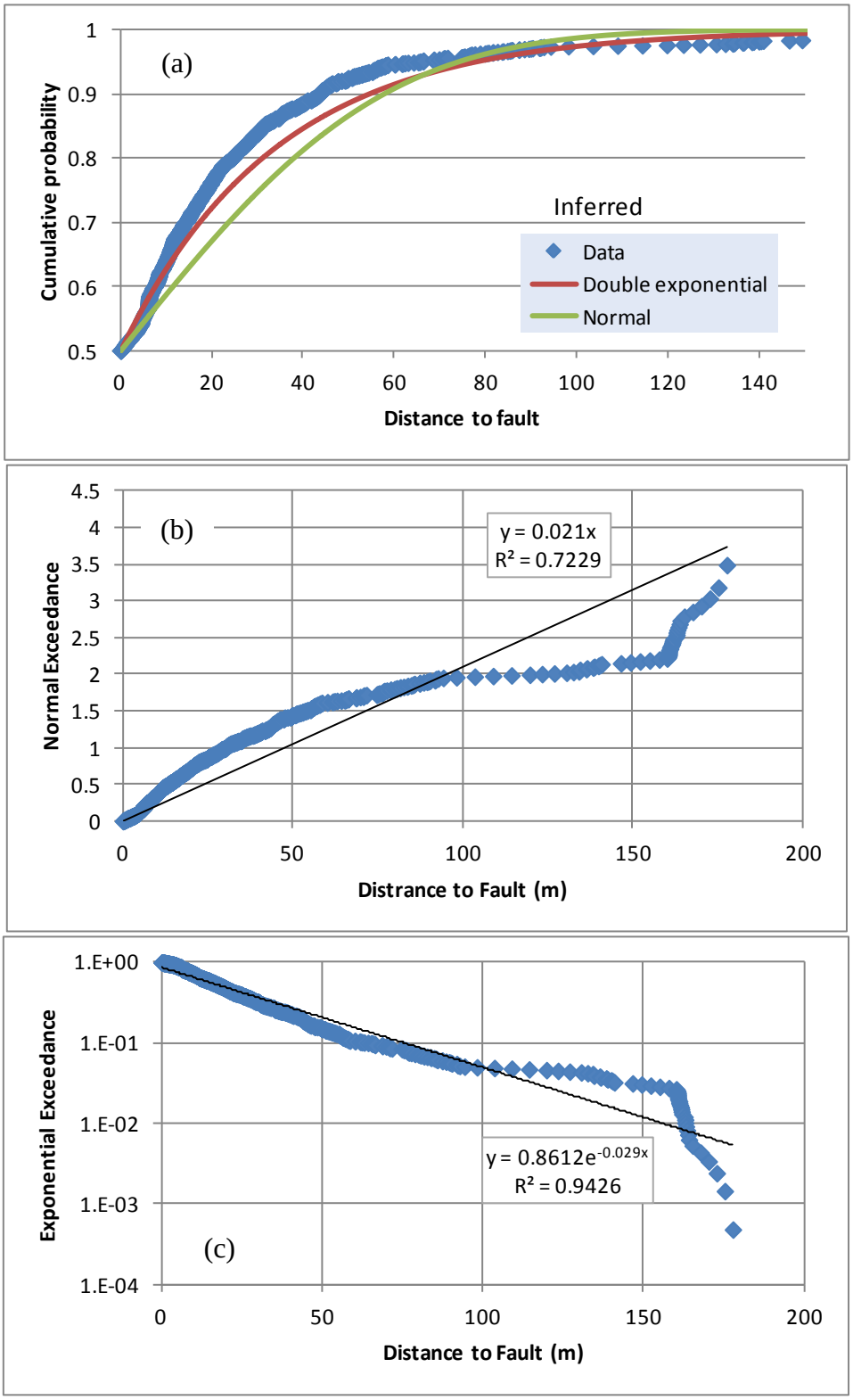

Figure 14. Comparison of inferred fault distance data combining all faults/fault segments: a. data cumulative distribution compared to theoretical normal and exponential cumulative distributions; b. exceedance plot for normal distribution; c. exceedance plot for exponential distribution.

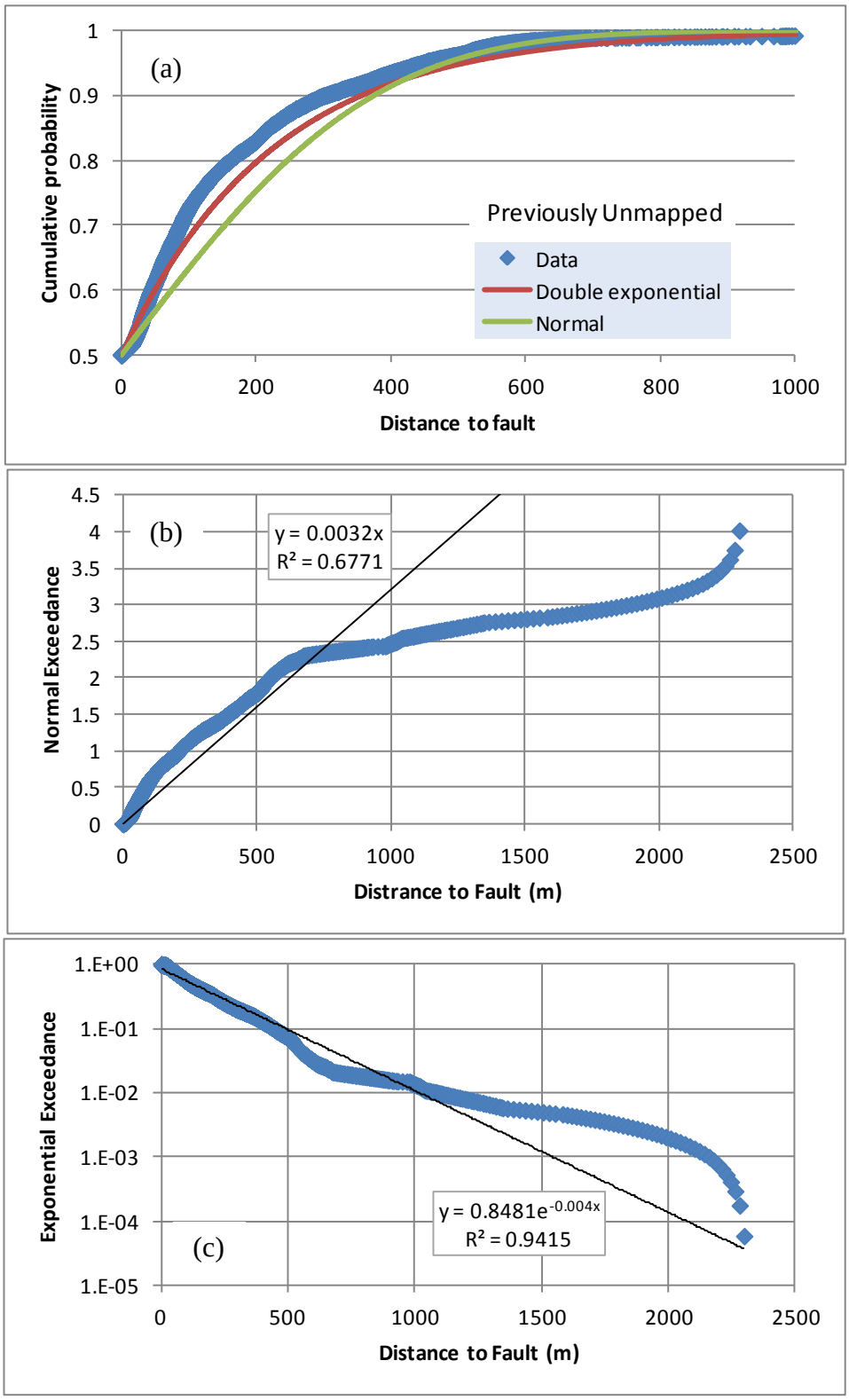

Figure 15. Comparison of previously unmapped fault distance data combining all faults/fault segments: a. data cumulative distribution compared to theoretical normal and exponential cumulative distributions; b. exceedance plot for normal distribution; c. exceedance plot for exponential distribution.

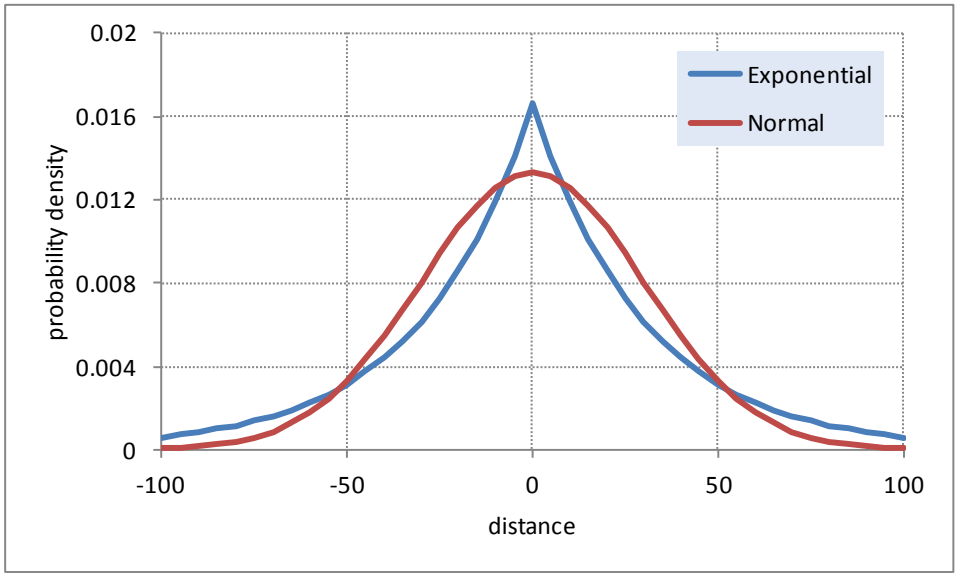

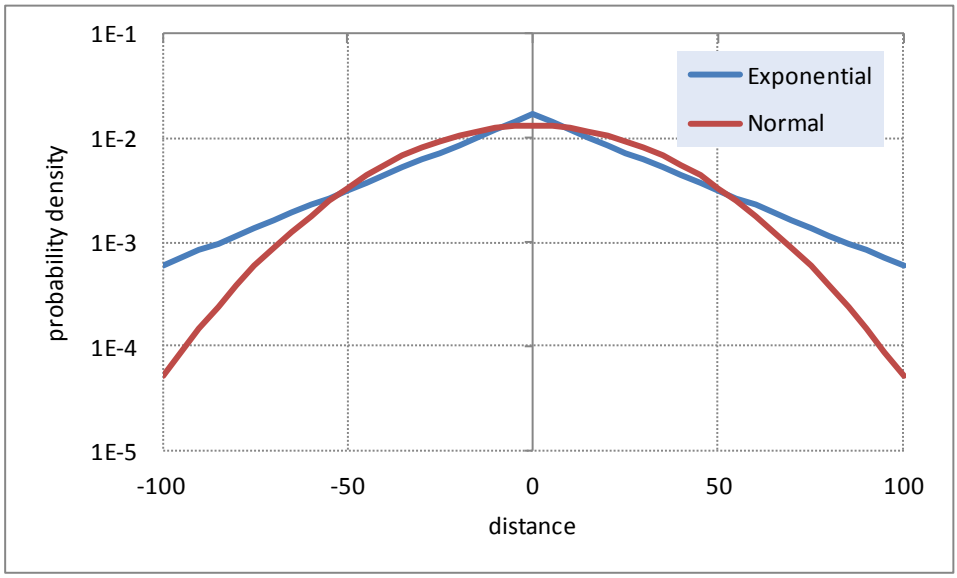

Figure 16. Comparison of probability density for normal and double exponential distributions: a. density curve in linear scale, b. density curves in log-linear scale. A standard deviation of 30 m is used for both distributions.

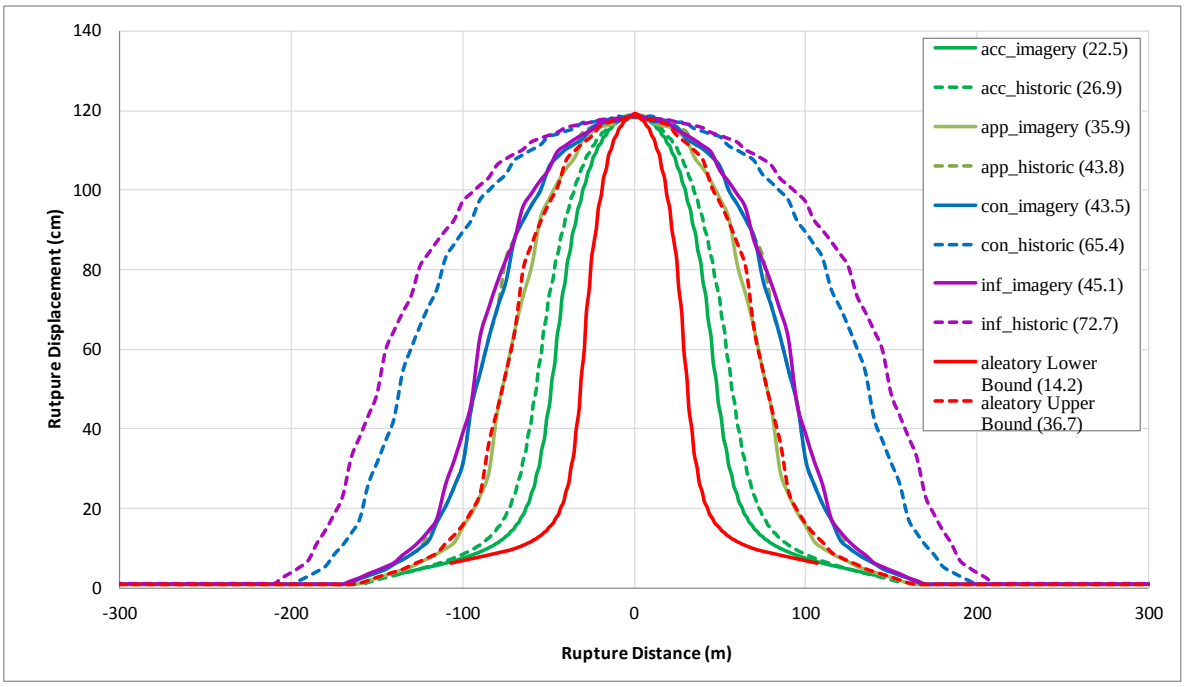

Figure 17. Comparison of displacement profiles across a mapped fault for a hazard level of 10% probability of exceedance in 50 years for different mapping quality categories based on quantifications of epistemic uncertainty from this study (imagery-based) and from Petersen et la. (2011) study (based on historical surface ruptures). Displacement profiles are also shown consider only aleatory location variability. The examples are for an M7.0 earthquake occurring once every 140 years. Other assumptions are described in the text.

Appendix A: Aleatory Location Variability Dataset

Mapped Trace Category	Trench Number	Trench Length (m)	Maximum Width of Faulting (m)	"Half Trench" Length (m)	Zone "Half Width" (m)	Event	Event Zone Width (m)	MRE Trace to Event Distance (m)	Comments	Citation
ACC	BDT4 NW	37	12.9	19	12.9	1 (BDT4a)	11			Ackiz et al. (2009)
ACC	BDT4 NW	37				2 (BDT4b)	3	6.2		Ackiz et al. (2009)
APP	3	175	114	175	114				Soil and bedrock. Other trenches at site not compiled (too short)	AP sites
APP	1	137	15	137	15				Trench mostly in bedrock. Note that main strand of mapped RCF not crossed by trench, but is a couple meters to the east of the east end of trench. Other trenches at site too short to be useful.	AP sites
APP	2	25	18	25	18				See previous comments.	AP sites
ACC	1	76	4.5	53	4.5				Trench is mostly in bedrock, but fault cuts Quaternary deposits. 1 of 2 strands at site, other strand not trenched (obvious trace at base of scarp)	AP sites
CON	1	64	1	51	1				Mapped trace is concealed	AP sites
CON	1	27	4.6	13	4.6	1?			1 event?	AP sites
CON	2	45	7.6	22	7.6				1 event?	AP sites
CON	3	27	6	24	6				Possibly more than one event.	AP sites
ACC	2	35	1.4	16	1.4				Soil and bedrock exposed.	AP sites
ACC	3	40	2.1	20	2.1					AP sites
ACC	4	40	1	20	1					AP sites
ACC	5	43	10	20	10					AP sites
ACC	1	27	7	19	7				Trench extends in only one direction away from fault.	AP sites
ACC	1	41	7.6	25	7.6					AP sites
ACC	1	36	1	18	1				Probably creeping trace	AP sites
ACC	-4 (compos	24	1	19	1				Single trace. Exposure is a composite of three trenches	AP sites
APP	1	49	3.4	39	3.4					AP sites
APP	1	73	1	49	1				Generally flat lying alluvium	AP sites
APP	3	75	3.8	45	3.8				Generally flat lying alluvium	AP sites
APP	1	21.3	6.1	16	6.1				in alluvium	AP sites
APP	2	16.8	4.9	10	4.9					AP sites
APP	T1-99	18.3	1	12	1				Possible creeping trace. Material called "Quaternary alluvium"	AP sites
APP	1	64	7.3	61	7.3				Mostly exposes steeply dipping bedrock	AP sites
APP	2	27	2	20	2				Faults flat-laying alluvium against steeply dipping bedrock	AP sites
ACC	/2 (composi	52	1	39	1					AP sites
ACC	WLA-1	29	2	20	2					AP sites
APP	2	76	19.5	53	19.5				Width based on reported "deformation zone"	AP sites
APP	3	27.4	5.8	19	5.8					AP sites
APP	98-3	60	9	60	9				Exposes Irvington gravels	AP sites

Mapped Trace Category	Trench Number	Trench Length (m)	Maximum Width of Faulting (m)	"Half Trench" Length (m)	Zone "Half Width" (m)	Event	Event Zone Width (m)	MRE Trace to Event Distance (m)	Comments	Citation
APP	1	32	1	22	1				Trenches expose decomposed bedrock. Total trench length is effective length from offset trenches.	AP sites
APP	2	32	4	22	4				Trenches expose decomposed bedrock. Total trench length is effective length from offset trenches.	AP sites
APP	2	17	3	9	3				Total trench length is effective length from offset trenches.	AP sites
APP	3	32	4.5	29	4.5					AP sites
APP	4	20	10.7	14	10.7					AP sites
APP	93-3	19	11	19	11	1	3		Probable MRE identified.	Reheis (1995)
APP	1	30	3.4	24	3.4					AP sites
APP	2	12	4	6	4				Trench length a composite from other trenches.	AP sites
ACC	1 and 2	51	6	30	6				Trace originally mapped as concealed?	AP sites
APP	1 and 2	120	1	100	1					AP sites
ACC	SPBT-1	25	1	14	1					Kelson et al (2000)
APP	1	44	2	12	2					AP sites
ACC	1	53	22	40	22				Weak shearing and slickenlines observed at max extent of faulting. One apparent major fault at station 1-1.	AP sites
ACC	A	35	1	27	1					AP sites
ACC	1	15	2	7	2	1	1			Lienkaemper and Williams (1999)
ACC	1	15				2+	2	1		Lienkaemper and Williams (1999)
ACC	1	25	1	12	1	creep?	1			Kelson et al (200X)
ACC	1	25				1?	1?	0.5		Kelson et al (200X)
ACC	5	6	1.5	5	1.5	1	1.5		Fault apparently reruptures narrow zone, creating colluvial wedges	Kelson et al (2006)
ACC	5	6				2	1.5		Fault apparently reruptures narrow zone, creating colluvial wedges	Kelson et al (2006)
ACC	5	6				3	1.5		Fault apparently reruptures narrow zone, creating colluvial wedges	Kelson et al (2006)
ACC	5	6				4	1.5		Fault apparently reruptures narrow zone, creating colluvial wedges	Kelson et al (2006)
ACC	5	6				5	1.5		Fault apparently reruptures narrow zone, creating colluvial wedges	Kelson et al (2006)
ACC	T1 and T3	33	12.5	25	12.5	T	4.5			Vaughan and Rockwell (1998)
ACC	T1 and T3	33				P	6.5?			Vaughan and Rockwell (1998)
ACC	T1 and T3	33				L	6.5			Vaughan and Rockwell (1998)
ACC	T1 and T3	33				H	12.5			Vaughan and Rockwell (1998)
ACC	1	12	5.1	9.6	5.1	many			39 m total lateral offset	Simpson et al (1998)
ACC	2	14	2	11	2	many			39 m total lateral offset	Simpson et al (1998)

Mapped Trace Category	Trench Number	Trench Length (m)	Maximum Width of Faulting (m)	"Half Trench" Length (m)	Zone "Half Width" (m)	Event	Event Zone Width (m)	MRE Trace to Event Distance (m)	Comments	Citation
ACC	T5	40	2.7	39	2.7	Z	1		T5 is selected as representative trench for the site.	Kelson et al. (1996)
ACC	T5		2.7			Y	1	1	T5 is selected as representative trench for the site.	Kelson et al. (1996)
ACC	T5		2.7			X	2	2	T5 is selected as representative trench for the site.	Kelson et al. (1996)
ACC	T5		2.7			W	2.4	2.7	T5 is selected as representative trench for the site.	Kelson et al. (1996)
ACC	"main"	20	3	20	3				Individual event information available, but very complex	Rockwell et al (1986)
APP	1	23	9.5	17	9.5	1	9.5			Rubin and Sieh (1997)
APP	1	23				PEN	7.5			Rubin and Sieh (1997)
APP	1	20	4.5	10	4.5	1	2.8			Hitchcock et al. (2001)
APP	1	20				2	1.9			Hitchcock et al. (2001)
APP		50	2	20	2					Hitchcock et al. (2001)
ACC	04A	110	3.8			1	1		Trench 04A goes across the entire pond. Entries here are only for the west trace, and do not include east strand (not sure how to correlate events from east to west side)	Lienkaemper and Williams (2008)
ACC	04A	110				2	0.6		Trench 04A goes across the entire pond. Entries here are only for the west trace, and do not include east strand (not sure how to correlate events from east to west side)	Lienkaemper and Williams (2008)
ACC	04A	110				3	0.55		Trench 04A goes across the entire pond. Entries here are only for the west trace, and do not include east strand (not sure how to correlate events from east to west side)	Lienkaemper and Williams (2008)
ACC	04A	110				4	3.4		Trench 04A goes across the entire pond. Entries here are only for the west trace, and do not include east strand (not sure how to correlate events from east to west side)	Lienkaemper and Williams (2008)
ACC	04A	110				5	3		Trench 04A goes across the entire pond. Entries here are only for the west trace, and do not include east strand (not sure how to correlate events from east to west side). Event zone width assumes full width of zone.	Lienkaemper and Williams (2008)

Mapped Trace Category	Trench Number	Trench Length (m)	Maximum Width of Faulting (m)	"Half Trench" Length (m)	Zone "Half Width" (m)	Event	Event Zone Width (m)	MRE Trace to Event Distance (m)	Comments	Citation
ACC	04A	110				6	3		Trench 04A goes across the entire pond. Entries here are only for the west trace, and do not include east strand (not sure how to correlate events from east to west side). Event zone width assumes full width of zone.	Lienkaemper and Williams (2008)
ACC	04A	110				7	3		Trench 04A goes across the entire pond. Entries here are only for the west trace, and do not include east strand (not sure how to correlate events from east to west side). Event zone width assumes full width of zone.	Lienkaemper and Williams (2008)
ACC	04A	110				8	3.2		Trench 04A goes across the entire pond. Entries here are only for the west trace, and do not include east strand (not sure how to correlate events from east to west side). Event zone width assumes full width of zone.	Lienkaemper and Williams (2008)
ACC	04A	110				9	?		Trench 04A goes across the entire pond. Entries here are only for the west trace, and do not include east strand (not sure how to correlate events from east to west side). Event zone width assumes full width of zone.	Lienkaemper and Williams (2008)
ACC	04A	110				10	3.9		Trench 04A goes across the entire pond. Entries here are only for the west trace, and do not include east strand (not sure how to correlate events from east to west side). Event zone width assumes full width of zone.	Lienkaemper and Williams (2008)
APP	1SE97	35	2	24	2	1	1 - 2			Fumal et al. (2003)
APP	1SE97	35				2	1			Fumal et al. (2003)
APP	1SE97	35				3	1 - 2			Fumal et al. (2003)
APP	1SE97	35				4	1 - 2			Fumal et al. (2003)
APP	2	14	4	10	4	1	2		Single fissure	Fumal et al. (2003)
APP	6	35	2	24	2	1	1 - 2			Fumal et al. (2003)
APP	6	35				2	1			Fumal et al. (2003)
APP	6	35				3	1 - 2			Fumal et al. (2003)
APP	6	35				4	1 - 2			Fumal et al. (2003)
APP	1	35	2.5	17	2.5	1	1		Trenches 1 and 5 considered representative for this site.	Fumal et al. (2003)
APP	1	35				2	2		Trenches 1 and 5 considered representative for this site.	Fumal et al. (2003)
APP	1	35				3	3		Trenches 1 and 5 considered representative for this site.	Fumal et al. (2003)
APP	1	35				4	4		Trenches 1 and 5 considered representative for this site.	Fumal et al. (2003)
APP	1	35				5	5		Trenches 1 and 5 considered representative for this site.	Fumal et al. (2003)

Mapped Trace Category	Trench Number	Trench Length (m)	Maximum Width of Faulting (m)	"Half Trench" Length (m)	Zone "Half Width" (m)	Event	Event Zone Width (m)	MRE Trace to Event Distance (m)	Comments	Citation
APP	5	17.5	1	9	1	1	1		Trenches 1 and 5 considered representative for this site.	Fumal et al. (2003)
APP	5	17.5				2	1		Trenches 1 and 5 considered representative for this site.	Fumal et al. (2003)
ACC	1 & 4	369	8	221	8				Trench is a composite of T1 and T4.	AP Sites
ACC	1	195	57	187	57				Site appears to be in a step over between mapped traces	AP Sites
ACC	1	244	98	146	98					AP Sites
APP	1, 2, 3	171	168	171	168				Composite trench spans distance between primary mapped trace to fault seen in T2.	AP Sites
APP	1 (south)	152	6	131	6				Trench spans two mapped traces. Measurement here splits the trench into two halfs.	AP Sites
APP	1 (north)	152	1	152	1				Trench spans two mapped traces. Measurement here splits the trench into two halfs.	AP Sites
ACC	1	142	6	123	6					AP Sites
ACC	1	76	17	57	17					AP Sites
APP	1	36	21	27	21					AP Sites
APP	4	43	11	38	11					AP Sites
APP	5	91	22	82	22					AP Sites
CON	1	680	20	340	20					AP Sites
CON	2	27	4	24	4					AP Sites
CON	1	253	1	242	1					AP Sites
APP	1	43	21	40	21					AP Sites
ACC	1	103	1	103	1					AP Sites
ACC	1, 2	122	81	85	81				Trench composite of T1 and T2, with 25' of overlap removed.	AP Sites
APP	1	152	43	152	43					AP Sites
CON	1, 3	271	185	271	185				Fault zone 3 not well-expressed in T3, but observed in other trenches.	AP Sites
ACC	4	91	1	77	1					AP Sites
ACC		98	36	76	36					AP Sites
ACC	4	171	1	128	1					AP Sites
ACC	1	177	1	30	1					AP Sites
ACC	1	190	58	190	58					AP Sites
ACC	2	238	17	232	17					AP Sites
ACC	1, 2, B	335	54	167	54				Trench 1, 2, composite	AP Sites
ACC	B	167	54	109	54					AP Sites
ACC	1	282	4.3	274	4.3					AP Sites

Mapped Trace Category	Trench Number	Trench Length (m)	Maximum Width of Faulting (m)	"Half Trench" Length (m)	Zone "Half Width" (m)	Event	Event Zone Width (m)	MRE Trace to Event Distance (m)	Comments	Citation
APP	1	152	113	146	113					AP Sites
CON	1	73	1	67	1				Fault trace not previously mapped, but site is within A-P zone	AP Sites
ACC	1	109	91	104	91					AP Sites
APP	1	15	1	10	1				Only one mapped fault trace trenched on property.	AP Sites
ACC	1	24	6	17	6				No scale provided, measurements off of site map.	AP Sites
APP	1A	73	13	57	13					AP Sites
APP	1B	80	20	80	20					AP Sites
APP	T2	65	20	37	20					AP Sites
APP	T3B	66	30	40	30					AP Sites
APP	1	98	1.2	90	1.2					AP Sites
APP	1	116	14	116	14					AP Sites
ACC	N	73	6	62	6					AP Sites
ACC	S	34	21	24	21					AP Sites
ACC	TP-3	150	105	127	105					AP Sites
APP	1	130	1	117	1					AP Sites
ACC	1	149	5.5	134	5.5					AP Sites
ACC	1	481	125	390	125				East trace not previously mapped. Other trenches on property, most are locator trenches.	AP Sites
ACC	9	82	17	68	17					AP Sites
ACC	10	46	13	23	13					AP Sites
ACC	11	27	6	13	6					AP Sites
ACC	1	16	1	15	1					AP Sites
CON	A	127	3	95	3					AP Sites
CON	B	35	2.4	18	2.4					AP Sites
APP	2	61	1	43	1				Fault is a secondary strand to the primary mapped trace located ~50 m to the east.	AP Sites
APP	A, B, C	126	6	126	6					AP Sites
CON	T1	908	12	454	12				Longest trench across site, other trenches mostly short locator trenches.	AP Sites
CON	T22	57	1	40	1				Additional possible folding over 25 feet observed in trench.	AP Sites
APP	1	255	10	192	10					AP Sites
APP	2	170	22	122	10					AP Sites
APP	11	316	17	180	17					AP Sites

Mapped Trace Category	Trench Number	Trench Length (m)	Maximum Width of Faulting (m)	"Half Trench" Length (m)	Zone "Half Width" (m)	Event	Event Zone Width (m)	MRE Trace to Event Distance (m)	Comments	Citation
ACC	1A/B	230	145						No primary fault, lots of older deformation mixed with younger deformation.	AP Sites
CON	1	570	48	285	48					AP Sites
CON	1, 2	84	51							AP Sites
CON	A, B103	103	13	90	13					AP Sites
ACC	1	130	1	21	1				This site is about 100 m from nearest mapped trace.	AP Sites
ACC	TR-3	85	11	85	11				Only east side of fault trenched.	AP Sites
APP	TR-2	61	3	30	3					AP Sites
APP	TR-2D	15	4.6	7	4.6					AP Sites
APP	TR-2E	15	4.6	7	4.6					AP Sites